DYNAMIC ENVIRONMENTAL TRANSMISSION ELECTRON MICROSCOPY

BY

JOCELYN CHU LAI

THESIS

Submitted in partial fulfillment of the requirements
for the degree of Master of Science in Materials Science and Engineering
in the Graduate College of the
University of Illinois at Urbana-Champaign, 2017

Urbana, Illinois

Adviser:

Ivan Racheff Professor Jian-Min Zuo
Assistant Professor Renske Van der Veen

ABSTRACT

The development of a dynamic environmental transmission electron microscope (DETEM) at the University of Illinois Urbana Champaign is documented in this thesis. The proposed apparatus is the first of its kind, combining the power of high-resolution electron imaging and diffraction of TEM, the time resolution provided by pulsed laser, and the in-situ capabilities of environmental transmission electron microscopy (ETEM) while also providing fast imaging capability using a CMOS pixel sensor for direct electron detection and a photoelectron gun. When operated in continuous imaging mode, the time resolution of the DETEM will be at least a factor of 30 larger than conventional electron microscopes. With the pulsed laser, dynamic events of reversible and irreversible processes in materials can be imaged and recorded with either stroboscopic or single-shot movie-mode methods. To develop the DETEM the Hitachi H-9500 300 kV TEM installed at the Frederick Seitz Materials Research Laboratory, has been modified to accommodate the optics to allow various pump-probe methods to take place for in-situ experiments. The design and assembly of the pump and probe optical inserts are described, along with the optical layout and its alignment that delivers the pump and probe laser beams. Characterization of the nanosecond pulsed laser system being implemented for the DETEM and ex-situ measurements of power threshold were also performed and recorded.

ACKNOWLEDGEMENTS

I would like to thank my professors, Jian Min Zuo and Renske van der Veen, for their constant support, guidance, patience, and faith in me throughout this project. My partner, Allan Sykes, who joined the project Fall 2016 and has been extremely helpful in being able to bounce ideas off with since I was no longer a lone wolf on the project. My prior teammates, Hyuk Park and Brittany Hagler, for bringing me up to speed over Summer 2016. My research group (Zuo Group) for their support, even though my project did not overlap with any of theirs, they were always willing to lend an ear whenever I was stuck with an obstacle.

TABLE OF CONTENTS

CHAPTER 1 INTRODUCTION 1
1.1 Motivation 1
1.2 Current Technologies of Time Resolved TEM 3
1.3 Application of TEM Techniques 5
1.3.1 Pump-Probe Method 5
1.3.2 Single-Shot Method 6
1.3.3 Movie-Mode Method 7
1.4 Dynamical Environmental TEM (DETEM) Project at UIUC 8
1.5 Thesis Organization 10
CHAPTER 2 DESIGN OF OPTICAL DELIVERY SYSTEM FOR DETEM 11
2.1 The Hitachi H-9500 & Gas Handling 11
2.2 Planned Dynamic TEM Operation Schemes 13
2.2.1 Fast Camera Only 13
2.2.2 Single-Shot Pump / Fast Camera Probe 13
2.2.3 Single-Shot Pump / Movie-Mode Probe 14
2.2.4 Single-Shot Pump / Single-Shot Probe 14
2.2.5 Nanosecond- and Femtosecond-Resolved Stroboscopic Pump Probe 15
2.3 Pump Delivery System Design 15
2.4 Cathode Delivery System Probe Design 18
2.5 Synchronization of Instruments 20
2.6 Laser Optical Table Setup 20
CHAPTER 3 CHARACTERIZATION OF OPTICAL SETUP 23
3.1 Laser Power Characterization 23
3.2 Doubling the Laser and using a BBO Crystal 26
3.3 Beam Size Measurement at the Sample Position 27
3.4 Theoretical Pump-Probe Overlap in the TEM 30
3.5 Communication between BNC Digital Delay Generator and VGEN Laser 31
3.6 Single-Shot Operation and Ex-Situ Testing with Quantifoil 35
CHAPTER 4 CONCLUSION AND OUTLOOK 41
REFERENCES 42
APPENDIX A – UPDATED LASER POWER MEASUREMENTS 46
APPENDIX B – TTL SIGNAL D25 52
APPENDIX C – BNC DDG TRIGGER SETTINGS 54

CHAPTER 1

INTRODUCTION

1.1 Motivation

Time resolved imaging was inspired by stop-motion photography, pioneered by photographer Eadweard Muybridge in 1872. He was curious about whether or not all four hooves of a trotting horse (see Figure 1) were simultaneously out of contact with the ground at any point in its stride [1]. By taking photographs with cameras with shutters triggered sequentially by a clockwork mechanism for regularly spaced photographs in time, entire sequences of motion could be obtained.

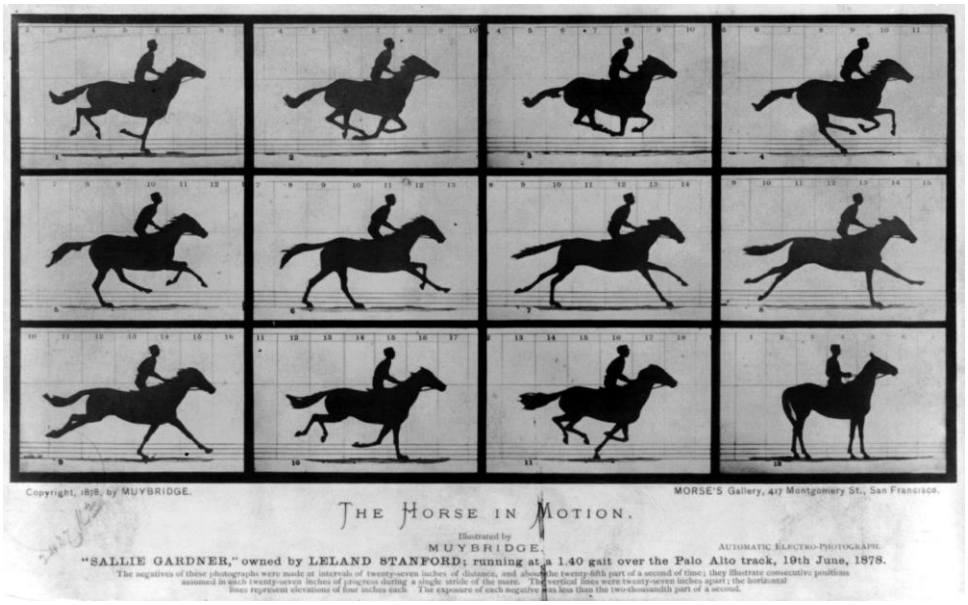

Figure 1. Early images studying motion of a running horse, proving that all four legs of a horse are completely off the ground at one time. Taken by E. Muybridge (1878). Image from Library of Congress [2].

Spark photography used short light flashes to expose an object moving in the dark to be visible to a detector during the light pulse, acting as the opening of a camera shutter. Greatly advanced by Harold Edgerton, a professor at MIT and cofounder of EG&G electronics, he released many iconic photos such as the falling apple and bullet through an apple Figure 2 [1]. Although these images were resolved on the millisecond time scale, with the appropriate detector and optics a well-resolved image of a specimen can be produced in principle to the nanosecond and femtosecond time scale.

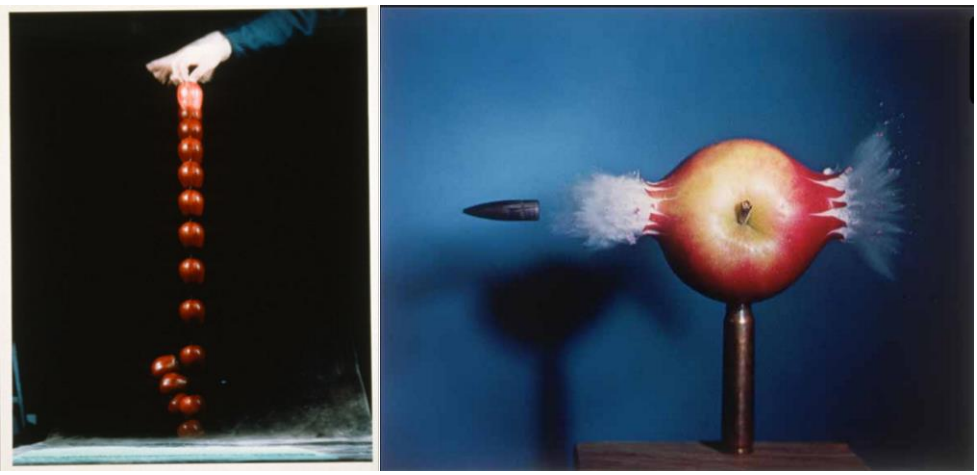

Figure 2. Iconic images apple drop (left) and bullet through apple (right) by Harold Edgerton, published in "Stopping Time" in 1987 [3, 4].

The transmission electron microscope (TEM) is a powerful tool that enables the visualization of atoms with length scales smaller than the Bohr radius at a factor of 20 times larger than the relativistic electron wavelength of 2.5 picometers at 200 keV [5]. This ability is largely due to the efforts made in correcting the imperfections in the lens systems that introduce aberrations and limit the achievable spatial resolution [6, 7, 8, 9]. With its capabilities, the TEM can directly map most of the properties of a material, including the composition, structure, bonding, morphology, and defects. However, because of the constant improvements with the lens systems, high resolution visualization of structural changes on the sub-millisecond time scales was not possible until recently [5].

In conventional TEMs, the spatial resolution is determined by the maximum spatial frequency of the electron wave transferred by the optical system, or the diffraction limit [10]. The specimen is illuminated with a plane electron wave, and the direct image formed by the objective lens is recorded in the image plane. Electrons are produced by either heating a source (thermionic emission) or by applying a strong extraction field (field emission), both of which result in the stochastic emission of electrons [5, 11]. In the stochastic emission of electrons, there is no control over the temporal spacing or relative arrival time at the specimen. Because of this, the spatial and temporal resolutions possible with short intense pulses with a large number of electrons in each pulse are limited to tens of nanometers and nanoseconds due to Coulomb repulsion.

Therefore, there is a constant trade-off in retaining high spatial resolution while simultaneously enabling temporal resolution to visualize atomic-scale motions.

Increasing the time resolution of the TEM allows for the study of fast, complex dynamical processes such as nanoparticle growth [12], phase transitions [13], self-assembly [14], dislocation dynamics [15] and nanomechanical motion [16] through direct *in situ* observation. The mapping in time of dynamical trajectories unravels key features of the forces of motion and associated effective and reduced energy landscape of structural dynamics [17]. With conventional cameras, there is a limit to imaging slow processes at ~30 ms time resolution, the standard readout for conventional charge-couple-device (CCD) cameras. There are two major implementations for increasing the time resolution in TEM – single-shot dynamic TEM with nanosecond resolution and stroboscopic pump-probe TEM with femtosecond-nanosecond time resolution. Both implementations rely on triggering fast dynamics in the material using a laser pulse prior to probing at later times.

1.2 Current Technologies of Time Resolved TEM

The very first dynamic TEM was invented by Bostongjolo and his group at the Technische Universität Berlin in 2000. They were the first to interface excitation and probe laser beams with a TEM, recognizing that high speed electron microscopy was capable of tracking fast laser-induced processes in metals below the ablation threshold [18] and imaging these processes on the time scale of nanoseconds. A standard 100 kV microscope was used with a self-built large top-entry specimen chamber housing a lens and a mirror for focusing the treating laser beam onto the specimen plus a fast electron beam blanker [3].By combining electron optics, fast electronics, and pulsed lasers, a transmission and a photoelectron emission microscope were built with the capabilities of 100 nm spatial resolution at 10 ns [18].

In 2005, Zewail *et al.* developed the first ultrafast electron microscope (UEM) at the California Institute of Technology, introducing the ability to nondestructively image complex structures with the spatial resolution of TEM as snapshots captured with ultrafast electron packets derived from a train of

femtosecond laser pulses [17]. This approach, also known as the stroboscopic approach, creates an image from many strobing packets that contain on average one electron per pulse and the specimen dose is a few electrons per square angstrom. By using coherent single-electron packets or a single electron bunch, coulomb repulse is absent, which permits imaging, diffraction, and spectroscopy with high spatiotemporal resolution [5]. At well-defined delay times after optical excitation, the evolving state of the sample is probed by an ultrashort electron pulse. The accumulation of many electron pulses yields a stroboscopic snapshot of the transient state of the system, where the transition state is repeatable [19].

Lawrence Livermore National Laboratory (LLNL) in Livermore, California designed and implemented a pre-existing JEOL 2000FX microscope to obtain an image of high resolution with a single electron pulse to study unique, irreversible events at nanosecond- and nanometer-scaled resolution [20], adopting the single-shot approach pioneered by Dömer and Bostanjoglo in 2003 [21]. The electron optical column has been modified to provide laser access to the photocathode and the specimen. This approach is also dubbed as dynamic TEM (DTEM), where time-resolved experiments are conducted by first initiating a transient state in the sample and then taking a snapshot of the transient process with a 15 ns electron pulse at some preferred delay after the initiation. The current configuration at LLNL can acquire images with better than 10 nm spatial resolution with 15 ns electron pulses [22]. The DTEM is also capable of providing multiple single-shot acquisitions (up to 9) in under ~1 μs, yielding frame rates on the order of 10^6 times higher than conventional *in situ* TEM frame rates[23]. Employing an arbitrary waveform generator to deliver a user-defined series of electron pulses of pulse duration and spacing [23], complex irreversible transformation events can be tracked across microsecond timescales, giving this method its name of move-mode DTEM.

More recently, the group led by Feist at the University of Göttingen in Göttingen, Germany developed the first ultrafast transmission electron microscope using a laser-triggered field emitter in 2016. Their instrument is based on a JEOL JEM-2100F TEM and modified to allow both optical sample excitation

and pulsed electron emission [19]. A new source was established for ultrafast TEM that employed localized linear photoemission from a nanometer-sized Schottky emitter, enabling operation with freely tunable temporal structure from continuous wave to femtosecond pulsed modes. The recorded pulse properties achieved were a 9 Å focused beam diameter, 200 fs pulse duration, and 0.6 eV energy width [19].

The aforementioned instruments are by no means the only instruments capable of time-resolved TEM experiments. There are many instruments that are currently in design and implementation phases for the capability of time-resolved TEM imaging.

1.3 Application of TEM Techniques

1.3.1 Pump-Probe Method

In time-resolved electron microscopy, the actual structure of materials can be obtained from pulses composed of high-energy or fast electrons, which have a wavelength on the same order of magnitude as interatomic distances. This is also known as the pump-probe technique [24]. The pulse that produces the spectrum, diffraction pattern, or image is the probe pulse. The probe pulse effectively "stops the motion" of atoms and obtains an instantaneous snapshot of the image of the molecular or materials structure. The motion captured by the probe is initiated by a clocking or pump pulse that triggers the dynamics. This establishes a temporal reference point of time zero for the changes that occur thereafter. Fixing the delay between the pump pulse and the probe pulse ensures precise capture of images of the dynamic evolving material. A successful image needs to have precise synchronization of the probe pulse sequence and a precisely defined launching configuration [1]. To synchronize the motion of many independent atoms or molecules to reach a similar point in structural evolution for the probe pulse, the relative timing of pump and probe pulses must be of femtosecond precision, and the launch of the configuration must be defined to sub-angstrom resolution in order for a relatively clear image to be created [1].

1.3.2 Single-Shot Method

The single shot approach was pioneered by Dömer and Bostanjoglo [21]. To obtain complete images from single-shot experiments, the TEM must operate at high current densities of 10^7 electrons per pulse or higher with minimal sacrifice of spatial and temporal coherence to extract information from the sample at an extraordinary rate. However, increasing the current density at the sample introduces space charge limits on spatiotemporal coherence in all TEM imaging as the local convergence angle α increases, which tends to wash out the image contrast. Single-shot DTEM adds an additional constraint that a single nanosecond-scale pulse must contain enough electrons (typically $\sim 10^7 - 10^8$) to provide an image of acceptable contrast and resolution [22]. Instead of just increasing spatial coherence by introducing apertures and adjusting condenser lenses and acquiring the image for a longer time, stringent requirements are placed for the brightness and current of the electron pulse. The brightness must be at least $\sim 10^7$ A $cm^{-2} \cdot sr^{-1}$ and the beam current must be on the millampere scale [22]. Furthermore, to keep the energy spread below 5 eV, the kind of electron sources that can be used is greatly reduced.

Electrons are charged fermions, meaning electron beams are subject to space charge effects, inhomogeneous scattering effects, and fundamental limits on spectral brightness, especially at extremely high current densities [22]. For very short pulses on the picosecond scale or faster, space charge effects can dramatically broaden both the duration and the energy spread of the pulse, degrading both spatial and temporal resolution [22]. Emittance is a measure of the phase space size and the brightness is a measure of how densely this phase space is filled, and a sufficiently flexible illumination system could allocate this phase space in just about any manner that would be desired, provided certain combinations of parameters are conserved. The performance of pulsed electron instruments is governed by the brightness of the electron source, especially for single-shot DTEM since it demands a very high fluence in a very short amount of time. Therefore, because of electron-electron scattering effects, microscope components and operating parameters must optimize the trade-off between spatial and temporal resolutions to achieve single-shot nanosecond- and nanometer-scale resolution [20].

With the single-shot technique, unique and irreversible events such as microstructural evolution, many solid-state phase transformations, and chemical reactions can be observed in the DTEM [25, 26, 27, 28, 29, 30, 31, 32, 33, 34].

1.3.3 Movie-Mode Method

Movie-mode DTEM refers to a technique where multiple single-shot acquisitions are captured in as little as ~1 μs, producing a frame rate nearly 10^6 times higher than that obtained by conventional in situ TEM [23]. First implemented at the Lawrence Livermore National Laboratory, this technique is designed to study processes for complex sequences of irreversible events that occur in a few microseconds. This method requires about 10^7 electrons per pulse, which amounts to beam currents in the range of milliamperes, which is orders of magnitude greater than the currents used in conventional TEM.

There are two ways to separate the individual images from electron pulses in a train. The first method is using a fast framing and highly specialized camera to capture each image between pulses. This method requires a camera with performance specifications that challenges the limits of current technologies. The second method is to install a high-speed deflector system between the sample and a standard TEM camera to deflect each pulse onto a different area of the camera, with an electronic timing system that switches deflection states in the time between electron pulses [23].

The movie-mode method was proved beneficial in observing the chemical reaction propagation fronts in reactive multilayer foils (RMLFs) [23], foils consisting of alternating layers of dissimilar metals and used for rapid, local application of heat for joining and fusing applications. However, with a single image frame per sample drive event, the entire film would be consumed and a new sample was needed for every time delay to be captured. By capturing multiple images as a single reaction front passes through the field of view, a single measurement of one sample could produce a data set with statistical power. This demonstrated the movie-mode ability to produce detailed quantitative information about complex nonequilibrium nanoscale phenomena.

1.4 Dynamical Environmental TEM (DETEM) Project at UIUC

The development of the Dynamical Environmental Transmission Electron Microscope (DETEM) at the University of Illinois Urbana Champaign was proposed as a versatile apparatus for time-resolved, in-situ, electron imaging and diffraction studies of fast material processes in gaseous and liquid environments through the introduction of a pulse laser driven photoelectron gun, a gas control system, and the integration of pulsed excitation for single shot and pump-probe measurements [35].

The DETEM will use a combination of a photoelectron gun, electro-optics and deflectors to achieve time resolutions from a few picoseconds to tens of nanoseconds. The photoelectron gun creates a pulsed electron beam when irradiated with short intense laser pulses, which can be arranged as "snapshots" of a dynamic event by deflecting individual electron images onto different parts of a detector to form a sequence of images. Repeatable processes are possible with the pump-probe approach to record a time series by initiating the process with a pulsed laser beam (the pump) and taking snap shots using a delayed electron beam as the probe.

Current designs are limited to imaging slow processes at video recording rates of about 30 frames per second, the standard readout for conventional charge-couple-device (CCD) cameras. Typical TEM imaging utilizes voltage and current densities on the order of 100-300 kV and 10^{-6}-10^{0} Acm^{-2}, which may generate secondary electrons from the sample, making analysis of chemical dynamics difficult when the secondary electrons produces a reactive radical. This makes the need for reducing electron beam effects and low dose electron imaging critical, where a microscope with intermittent pulsed excitation/acquisition and single electron detection is desired for the study of chemistry and the time domain of relevant reactions.

Major improvements have been made to the Hitachi H-9500 300 kV TEM with a LaB_6 emitter, the development platform for the DETEM, including the design and installation of a gas handling mixing system, a dual camera system with a Gatan Orius camera for video rate image recording and a K2 IS camera for direct electron detection and fast recording at 400 frames per second for full frame transfer or 1600

frames per second at ¼ frame transfer [36], and a high temperature sample heating holder up to 1500°C [37]. The improvement in time resolution was demonstrated in a heating experiment of Au catalyst on silicon nanowires (NW) [38]. At 2.5 ms apart when the Au catalyst was heated to 400 °C, initial movements of Au catalyst were observed (See Figure 3), followed by a significant change in the wetting angle of Au nanoparticle. Afterwards Au was seen diffuse away along the NW surface as indicated by fast image contrast change.

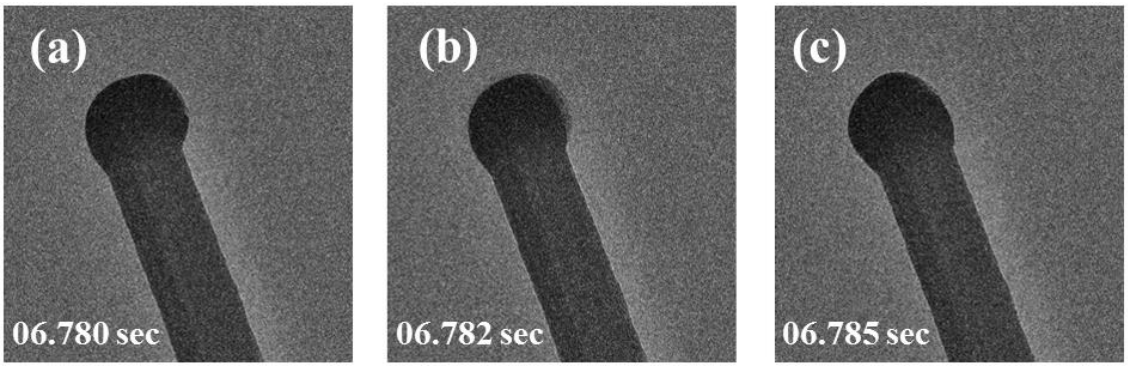

Figure 3. Au catalyst movements on a silicon nanowire captured by a fast direct detection electron camera. The time stamp on the bottom left corner of the images show frames captured into 6 seconds of observation with 2.5 ms time interval [38].

This proposed apparatus is the first of its kind, combining the power of high-resolution imaging and diffraction of TEM, the time resolution of DETEM, and the environmental control of environmental transmission electron microscopy (ETEM), while providing fast imaging capability by improving the time resolution of in-situ electron microscopy by a factor of 30 or more using a CMOS pixel sensor and the photoelectron gun [35]. The *in situ* environmental TEM allow for high resolution electron optics to function in controlled environments and enable observation and analysis of materials and chemical reactions under realistic conditions. The DETEM at UIUC features a custom-made CMOS monolithic active pixel sensors for direct electron detection for enhanced TEM detector resolution, with readout rates of about 400 frames per second, about ten times faster than typical CCD cameras. Although brighter electron sources will be required to ensure that a sufficient number of electrons is able to reach the sample for an image to appear, the photoelectron gun can be utilized to generate the electron packets needed for the desired brightness.

The DETEM at UIUC will be capable of functioning in a wide span of time resolutions, from milliseconds to femtosecond range, allowing a truly versatile range of applications to be observed in the DETEM.

1.5 Thesis Organization

This thesis has two main parts: the design of the optical delivery system and the characterization of the system. The design of the optical delivery system consists of the main techniques that the optical delivery system will utilize in its integration with the TEM, the TEM instrument being modified, and the optical components of the laser system modifying the TEM. The initial results consist of measurements taken to characterize the laser, calculations and schematics during the manipulation of the laser on the optical table, and the documentation of technical challenges during the development process.

CHAPTER 2

DESIGN OF OPTICAL DELIVERY SYSTEM FOR DETEM

2.1 The Hitachi H-9500 & Gas Handling

The Hitachi H-9500 is a 100-300 kV TEM with a LaB_6 electron gun. This user-friendly instrument is used for atomic-resolution TEM imaging and routine structural characterization with excellent imaging quality [39]. It is capable of 0.10 nm lattice resolution and 0.18 nm point-to-point resolution images with a stable 5-axis eucentric goniometer stage. A labeled schematic of the instrument and its lens configuration can be found in Figure 4.

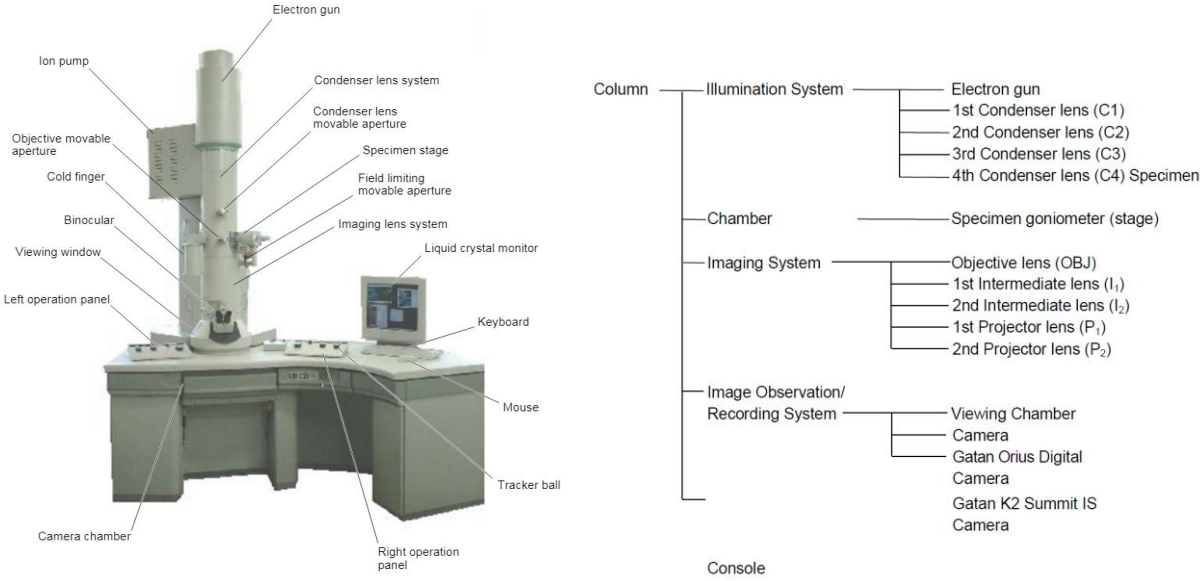

Figure 4. Labeled appearance of Model H-9500 (left) and lens configuration diagram inside the TEM (right) [40]

The Hitachi H-9500 has also been modified to be capable of environmental TEM in-situ experiments with a home-made gas handling system at UIUC, imaged in Figure 5. The gas handling system is composed of four gas tanks: O_2, CO, N_2, and H_2. The four gas tanks are connected to mechanical valves that enables users to open or close valves mechanically. The valves can also be manipulated digitally through a digital controller that is connected to the mechanical valves. From the mechanical valves, the gases selected are led to the sample chamber by means of a specific holder where a nozzle directs the gas

to the sample. Users can manipulate the digital controller through a software on the connecting laptop to control the flow rate, which is effectively the valve through the software, although timing must be done by user to start and stop the flow of gases. Users also have the ability to mix gases together into the sample chamber. The Hitachi H-9500 has a goniometer in the sample holder chamber to report the pressure of the chamber in the TEM.



Figure 5. Images of environmental gas-handling system that is connected to the Hitachi H-9500. The gas tanks containing O_2, CO, N_2, and H_2 are along the bottom of the cabinet, with gauges to show the pressure of the tanks themselves. The gas tanks are connected to mechanical valves, along the wall on the upper-right corner of the cabinet.

2.2 Planned Dynamic TEM Operation Schemes

2.2.1 Fast Camera Only

Fast camera operation consists of a continuous stream of electrons (the dotted lines in Figure 6) of increased brightness from the photocathode in order for better signal-to-noise ratio. A higher integrated pulse flux is present with the pump pulse timed with the set time-frame, where in Figure 6 indicates a time frame range of 400 Hz for full frame transfer or 1600 Hz at ¼ frame transfer [36]. The overall timescale of this scheme is around 2.5 ms.

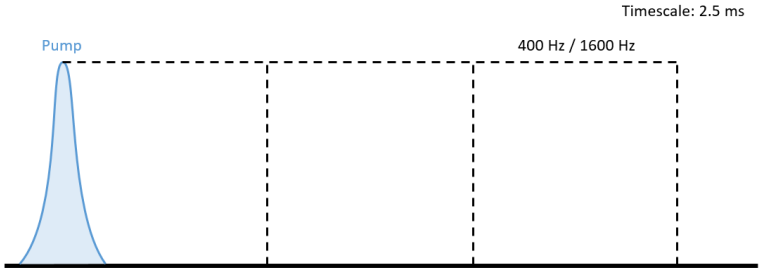

Figure 6. Fast camera schematic, where the dotted lines indicate the continuous stream of electrons from the photocathode.

2.2.2 Single-Shot Pump / Fast Camera Probe

The single-shot pump and fast camera probe adds a trigger to the laser pulses as a photon source or a thermal heat jump, with a continuous stream of electrons to probe (Figure 7). The timescale of this scheme is also at 2.5 ms.

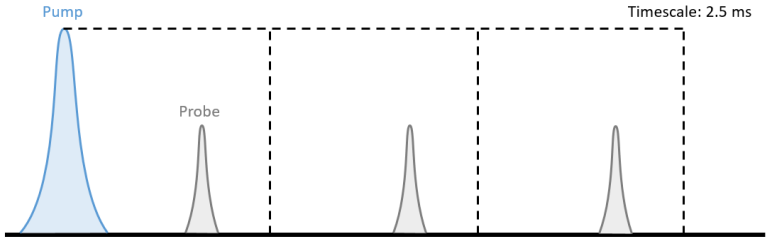

Figure 7. Single-shot pump and fast camera probe schematic, where the dotted lines denote a continuous stream of electrons. Note how the probe is repeating as it is triggered as a photon source or thermal heat jump.

2.2.3 Single-Shot Pump / Movie-Mode Probe

In this single-shot pump and movie-mode probe, a single-shot laser pulse is sent to the sample to trigger a material process, while also triggering 9 probe pulses from the cathode. The 9 probe pulses are deflected to show 9 separate images of one triggered material process across one continuous time frame (Figure 8). This scheme is on the time scale of about 100 µs.

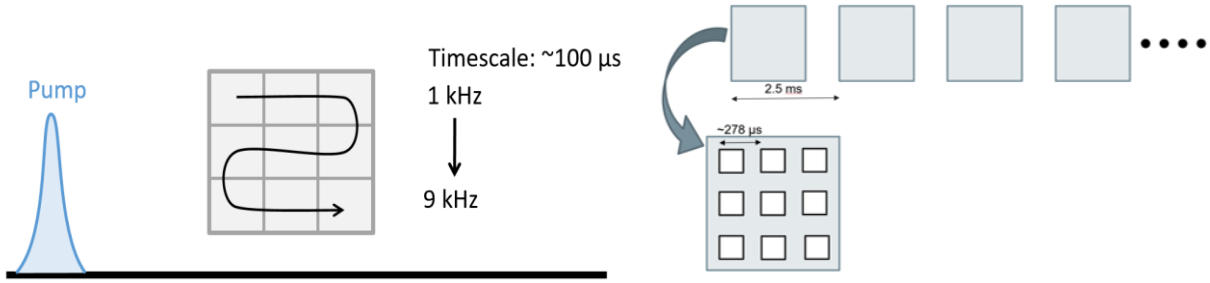

Figure 8. Schematic of pump and probe pulses for movie mode technique (left) and how a whole image is captured by deflection of multiple electron pulses (right).

2.2.4 Single-Shot Pump / Single-Shot Probe

The single-shot pump and single-shot probe scheme is used for a single instantaneous image of a material process that occurs on the nanosecond time scale (Figure 9). This scheme would be used for irreversible material processes, where the pump pulse and probe pulse are triggered and timed to image a specific instance during the desired material transition.

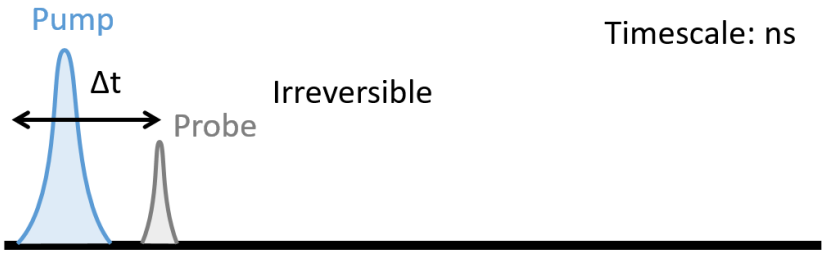

Figure 9. Schematic of pump and probe pulses for single-shot technique.

2.2.5 Nanosecond- and Femtosecond-Resolved Stroboscopic Pump Probe

The nanosecond- and femtosecond- resolved stroboscopic pump probe scheme will be for stroboscopic imaging of a reversible process, using a lower fluence but capturing parts of the same image being illuminated by the probe pulse at a specified time after the pump pulse (Figure 10). While the current laser is limited at 3 nanoseconds, there are current plans to purchase a femtosecond laser to allow for femtosecond resolution stroboscopy.

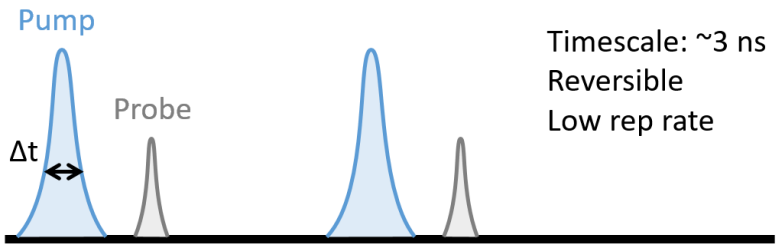

Figure 10. Schematic of pump and probe pulses for stroboscopic method.

2.3 Pump Delivery System Design

The design of the pump delivery system was based on the following concept constraints:

1. Adaptability for laser pulse lengths (ns, ps, fs) for future reference
2. Adjustability for focused beam positioning
3. Stable laser beam positioning with minimum vibration

A combination of mirrors capable of working with picosecond and femtosecond laser was used for future iterations or editions of the laser setup. The assembly was designed with two degrees of freedom of adjustable length and rotation of the insert for flexibility in laser beam alignment to the sample, depicted in Figure 13. Fiber optic cables are used to deliver the laser beam from the laser source to the pump delivery system right in front of the TEM to the sample for nanosecond laser pulse. A schematic of the behavior of the beam after the fiber and into the pump delivery system is shown in Figure 11. For flexibility to align the laser beam and electron beam at the sample position, a transmission lens and flat mirror assembly is designed with a commercially available lens and two flat mirrors.

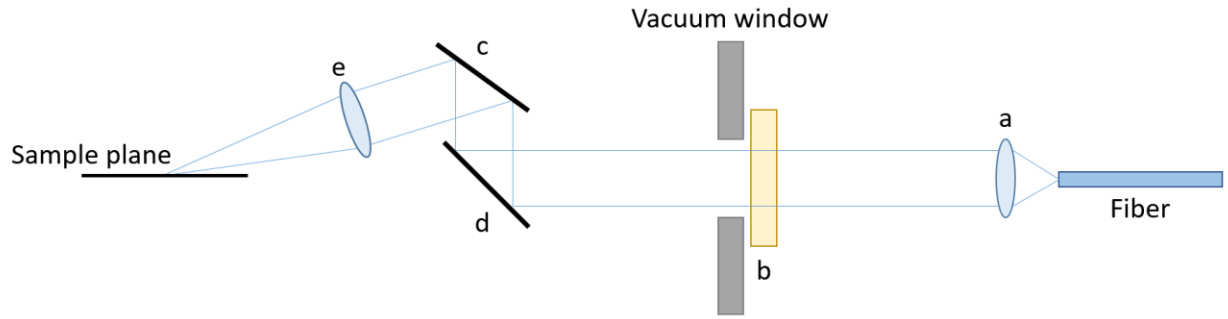

Figure 11. Ray diagram manipulation of light through the series of optics, where (a) is the fiber collimator optic (Thorlabs #CFC-11X-C), (b) is the viewport window (Thorlabs #WG41050-A), (c) is a 34°/56°/90° right angle mirror, (d) is a 45°/45°/90° right angle mirror, and (e) is the lens (Thorlabs #LA1222-A) inside the lens block, tilted 22° down from the horizontal to focus the beam onto the sample plane.

Alignment of the mirrors and the lens block is achieved with the use of a custom apparatus block made by Hyuk Park. The apparatus block was designed to make alignment possible for the bottom mirror (part d of Figure 11), top mirror (part c of Figure 11), and the lens block, in that order, to accurately align the beam towards a specific point on the sample plane, which is simulated through the use of a beam alignment plate. The 30 mm cage rods are used to guide the collimated beam from a single-mode optical fiber from a distance and for aligning the beam after it hits a mirror, where the angle of the beam being directed by the mirror determines the placement of the second set of 40 mm cage rods (Figure 12). The respective screws are adjusted for the mirror until the beam is aligned to the center of the alignment target.

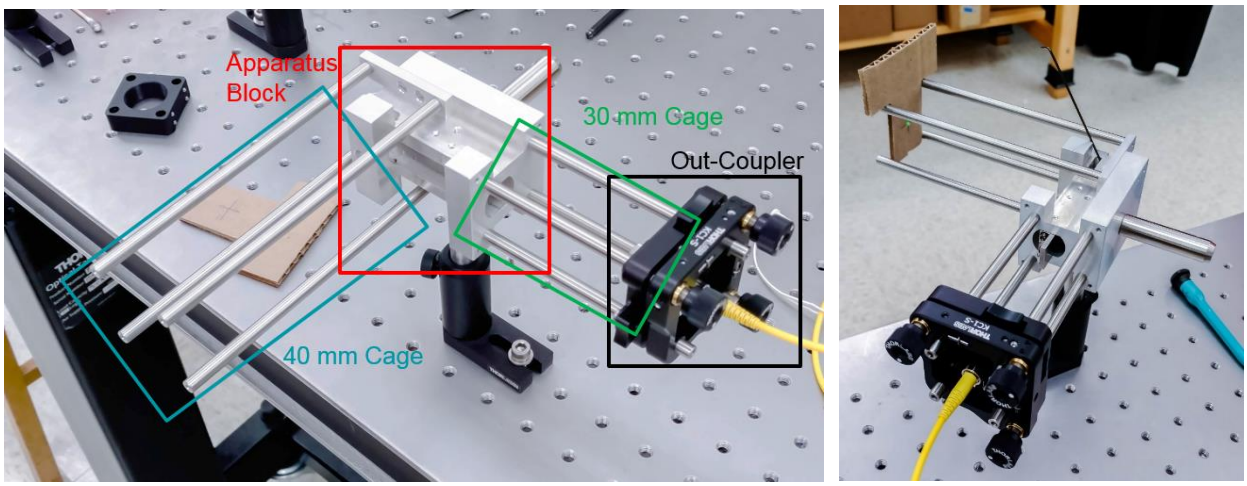

Figure 12. Apparatus block with 30 mm cage rods and 40 mm cage rods to hold the out-coupler and the target, respectively.

This alignment is done twice with the bottom mirror and then the top mirror, where the bottom mirror redirects the beam so that it is 90° upwards from the incoming beam, and the top mirror redirects the beam 90° again so that the outgoing beam is 180° from the incoming beam. Finally, the beam alignment plate is added to the pump delivery system to align the lens block with its linear adjustment so that the beam is directed and focused into the hole of the beam alignment plate. The final assembly of the pump delivery system with the beam alignment plate is depicted in Figure 14. The pump delivery system is currently housed in the Hitachi H-9500 sample chamber after alignment of the mirrors and shortly before Hyuk left the project in August 2016.

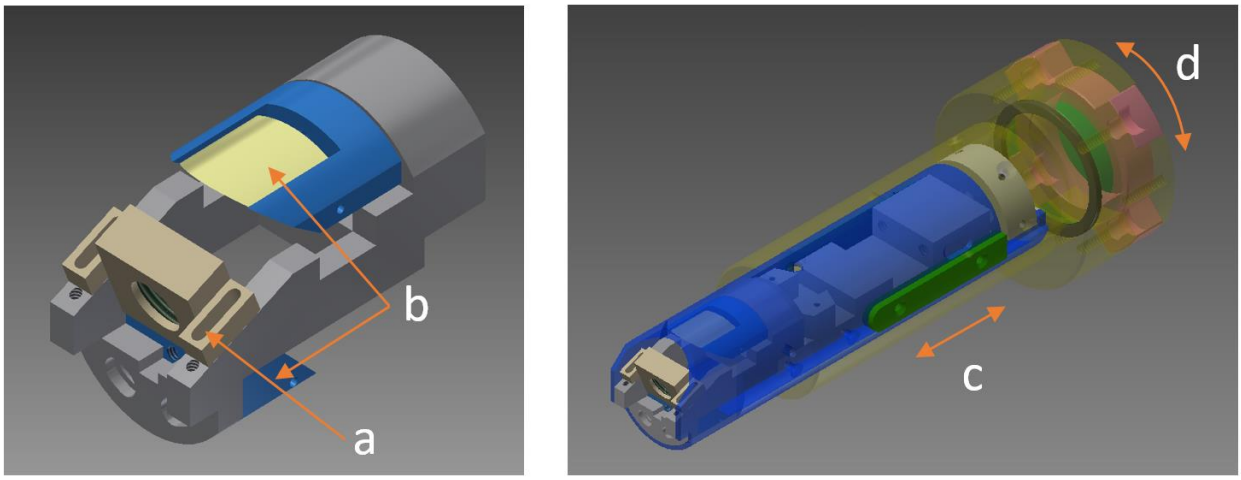

Figure 13. CAD of pump delivery system, with close-up of the mirror and lens assembly (left). Parts designed to be adjustable are labeled and pointed out, where (a) is the lens holder with linear adjustment, (b) points to the two mirrors that have two degrees of freedom, (c) show were the length can be adjusted, and (d) is capable of rotational angle up to a specific degree. [16]



Figure 14. Fully assembled pump delivery system with beam alignment plate

2.4 Cathode Delivery System Probe Design

The design of the cathode delivery system (see Figure 17) was based on the following constraints:

1. Maintaining performance of the TEM for conventional TEM imaging and diffraction
2. Easy maintenance
3. Easy alignment

To meet the above goals, a new column segment was designed for the insertion of the cathode delivery system and an extra viewport for monitoring (Figure 15). The design was made such that the mirrors could be replaced without taking out the electron gun column, with two degrees of freedom for each mirror.

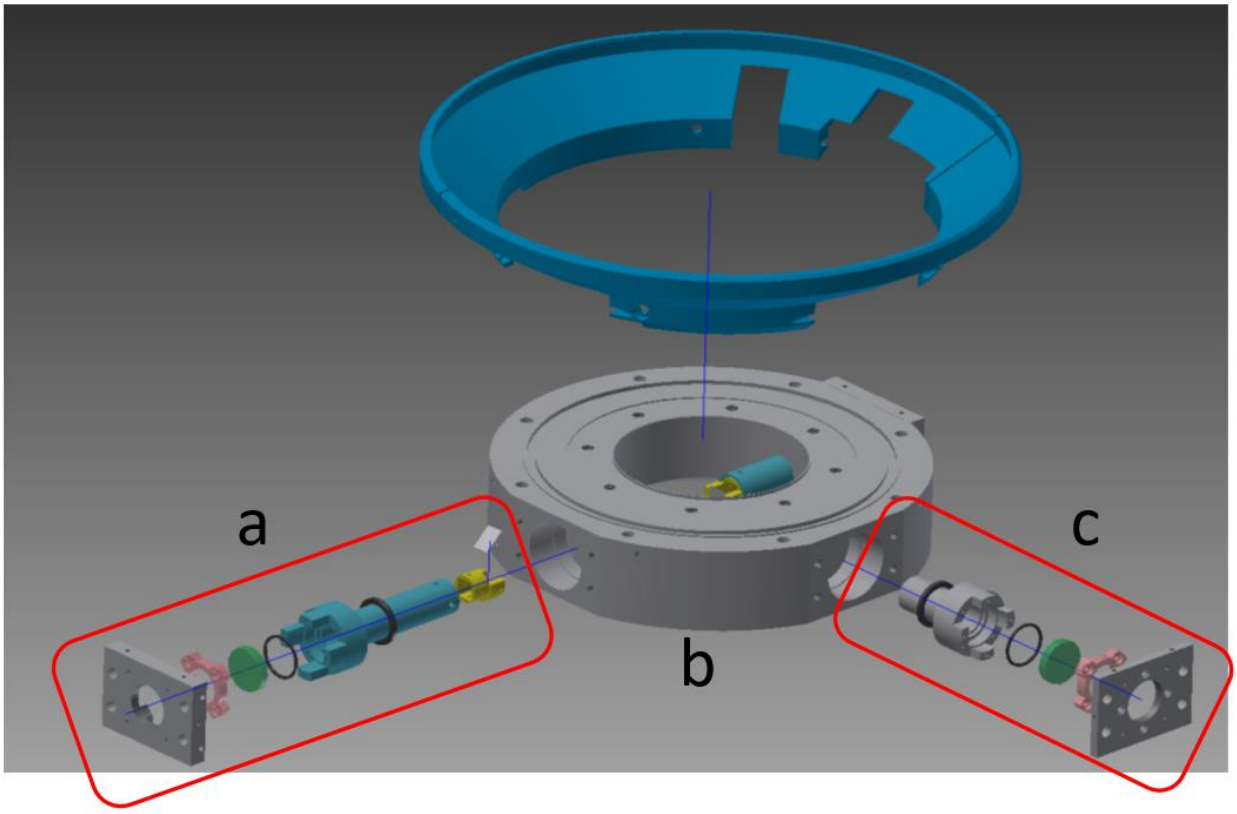

Figure 15. CAD of (a) cathode delivery system with (b) extension column and (c) extra viewport. This extension column is inserted in the Hitachi H-9500 above the condenser lenses but below the LaB_6 electron gun. [16]

The alignment for the cathode delivery system is simpler than that of the pump delivery system, since there is only one mirror needed to align. The alignment of the mirror in the cathode delivery system is much simpler than the alignment of the pump delivery system. There are two holes to hold the mirror in place from the sides, and two set screws with a rounded end located on the bottom of one side of the right-angle mirror to adjust the angle of the mirror. The mirror is aligned when it is flushed with the flat end of the helmet (see Figure 16).

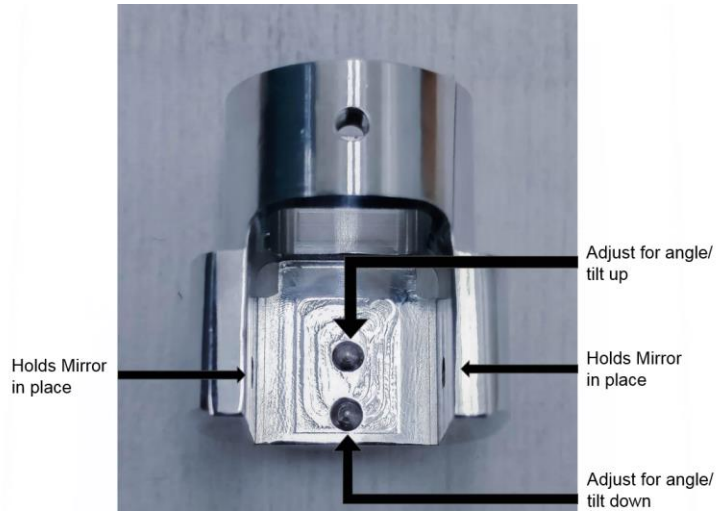

Figure 16. Helmet component of cathode delivery system where right angle mirror is placed and adjusted. Right-angle mirror omitted from image in order to see the set screws for adjustment and the placement of the set screws to hold the mirror in place.



Figure 17. Assembled cathode delivery system

2.5 Synchronization of Instruments

The interaction of the instruments can be organized together in Table 1, created by Hyuk Park.

Table 1. All the components and how they are connected together for DETEM [41]

Components	Signal	Connected as	Controlled by	Rep Rate(kHz)
K2 Camera	TTL	Master	Computer	0.4
ns Laser	TTL	Slave	Delay Pulse Generator	20 kHz
Pulse Picker 1 for pump laser	TTL	Slave	Delay Pulse Generator	Single
Pulse Picker 2 for Cathode Laser	TTL	Slave	Delay Pulse Generator	>0.4
Deflector	Ethernet	Slave	Computer	~1

All of the instruments are to be synchronized by a digital delay generator, with the master signal generated by the K2 camera used with the Hitachi H-9500. A single laser system (described more in detail in the next section) will be used as the pump and probe laser, integrated with two pulse pickers. Currently UIUC has magnetic deflectors that can only be controlled by the software through the internet, therefore the overall temporal resolution is limited by the speed of the magnetic image deflector.

There are current plans in purchasing a second laser for pump probe, which changes the above relationship between components so that the delay pulse generator would be used to change the relative delay between the pump and probe laser pulses.

2.6 Laser Optical Table Setup

The laser chosen for the pump and probe pulses is the VGEN (Spectra-Physics) laser Model VPFL-G-10-HE. This specific laser is a pulsed green fiber laser (532 nm) with nanosecond tunable pulse width from 3 to 20 ns and tunable repetition rate of single shot and up to 1500 kHz with up to 200 μJ pulse energy [42]. The laser is comprised of short-pulse, linearly polarized Ytterbium fiber lasers in master oscillator power amplifier (MOPA) configuration along with a second harmonic generation (SHG) module, providing

an output power of up to 30 W. Table 2 lists out important parameters of the VGEN laser as given by the VGEN User Manual [42].

Table 2. VGEN Laser Specifications (Model VPFL-G-10-HE)

PARAMETER	TEST CONDITION	UNIT	MIN	TYPICAL	MAX
Repetition rate (tunable		kHz	1		1000
Pulse width		nsec	3		20
Wavelength		nm		532	
M^2		[]			1.3
Polarization				Linear	
ON/OFF switching time	'Arm' to 'Active' states	μs			50
Output beam diameter	$1/e^2$	mm	2	2.5	3
Input voltage (factory setting)		V	20	24	27
Dimensions	Laser generator	mm	95 x 195 x 282		
	Optical head unit	mm	98x116x220 (with heat sink) 77x116x220 (without heat sink)		

The overall layout of the optics with the VGEN laser used for the optical delivery is outlined in Figure 18. The basic concept is that the original output of 532 nm wavelength by the VGEN laser is to be used as the pulses that act as the "pump" to the sample, exciting the sample to invoke the desired reaction. On the optical table, the 532 nm wavelength is doubled through a Type 1 BBO second harmonic generation (SHG) crystal (see Chapter 3.2) and a beam splitter (Thorlabs #HBSY134) is used to deflect the 266 nm wavelength light and couple the ultraviolet (UV) light into a fiber coupler for UV. The 532 nm wavelength light would pass through the beam splitter and redirected to a fiber coupler for 532 nm light. The 266 nm beam coupled into the UV fiber coupler would be directed to the cathode delivery system in the extension column of the Hitachi H-9500 while the 532 nm beam coupled into the 532 nm fiber coupler would be directed to the pump delivery system in the sample plane of the Hitachi H-9500.

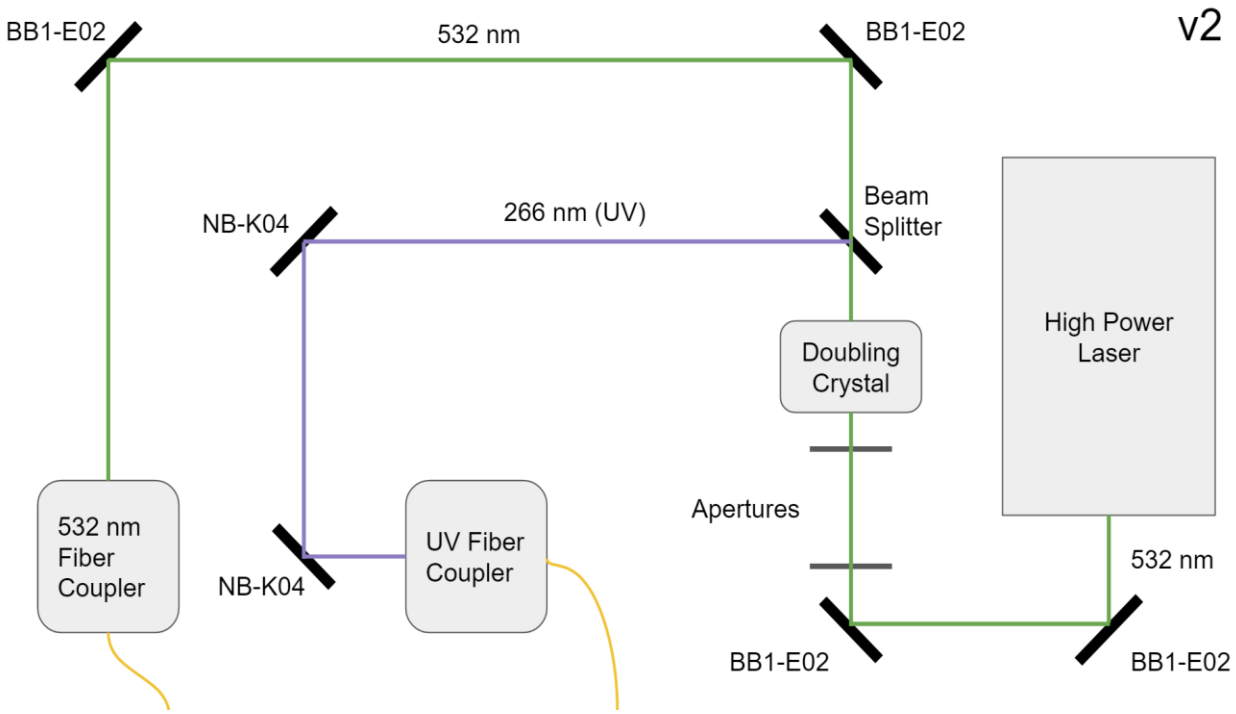

Figure 18. General optical table schematic with labeled optical components

CHAPTER 3

CHARACTERIZATION OF OPTICAL SETUP

3.1 Laser Power Characterization

One of the first measurements taken after setting up the optical table and aligning the optics was measuring the power of the laser. These measurements were taken as reassurance that the power values measured accurately reflected that of the specifications sheet provided by VGEN in its User Guide. The setup used to measure the power is shown in Figure 19.

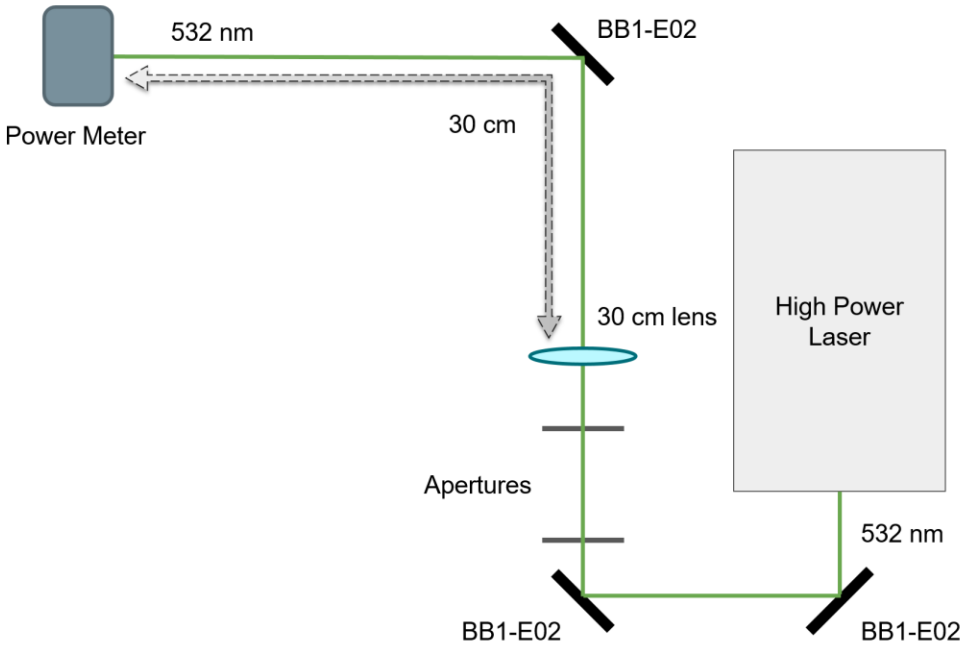

Figure 19. Power characterization optical setup

In this setup, a 30 cm focal length lens was used to focus the beam onto the power meter. The focal point beam diameter was calculated using Gaussian beam optics for the theoretical spot size area. The focused beam has a minimum diameter, called the beam waist, at the focal point.

The beam waist diameter ($2w_0$) is defined by Equation 1, reproduced below:

$$2w_0 = \left(\frac{4\lambda}{\pi}\right)\left(\frac{f}{D}\right) \qquad \text{(Equation 1)}$$

Where w_0 is the beam waist radius, f is the lens focal length, λ is the wavelength, and D is the input beam diameter. Plugging in the numbers, the diameter of the beam at its smallest is 81.28 μm.

$$2w_0 = \left(\frac{4(532\ nm)}{\pi}\right)\left(\frac{30\ cm}{2.5\ mm}\right) = 81.28\ \mu m$$

From the calculations, the radius of the beam at the power meter is $4.06*10^{-3}$ cm, corresponding with an area of $5.19*10^{-5}$ cm^2.

The Rayleigh length (z_R) is defined by Equation 2, which gives the length along the optical axis until the beam doubles in size from the focal point. This was first calculated for this setup as a starting point in understanding laser behavior and is more useful for BBO crystal placement in the next section.

$$z_R = \frac{\pi w_0^2}{\lambda} \qquad \text{(Equation 2)}$$

$$= \frac{\pi(4.06 * 10^{-3}\ cm)^2}{(532\ nm)} = 0.97\ cm$$

With the beam area, repetition rate (PRR), and pulse width, the measured power density can be calculated with the measured power from the power meter using Equation 3.

$$Power\ Density = \frac{\frac{Measured\ Power\ [W]}{Beam\ Area\ [cm^2]}}{PRR\left[\frac{1}{s}\right] * Pulse\ Width\ [s]} \qquad \text{(Equation 3)}$$

Measuring the power with the first two preset settings of the VGEN laser, labeled OPNUM (operational number) 0 and 1, the gain was incremented by 1 until the maximum possible gain and the measured power of the power meter was recorded. The preset parameters corresponding with OPNUM 0 and 1 are in Table 3.

Table 3. Laser parameters for preset settings of OPNUM 0 and 1.

OPNUM	0	1
PRR Max [kHz]	180	300
Pulse Width [ns]	3	3
Max. Avg power [W]	10	10
Pulse Energy [uJ]	55	33
Max Gain	53	59

The measured power across varying repetition rates were recorded and plotted for both OPNUM 0 and 1 for each increasing gain value, plotted in Figure 20 and Figure 21.

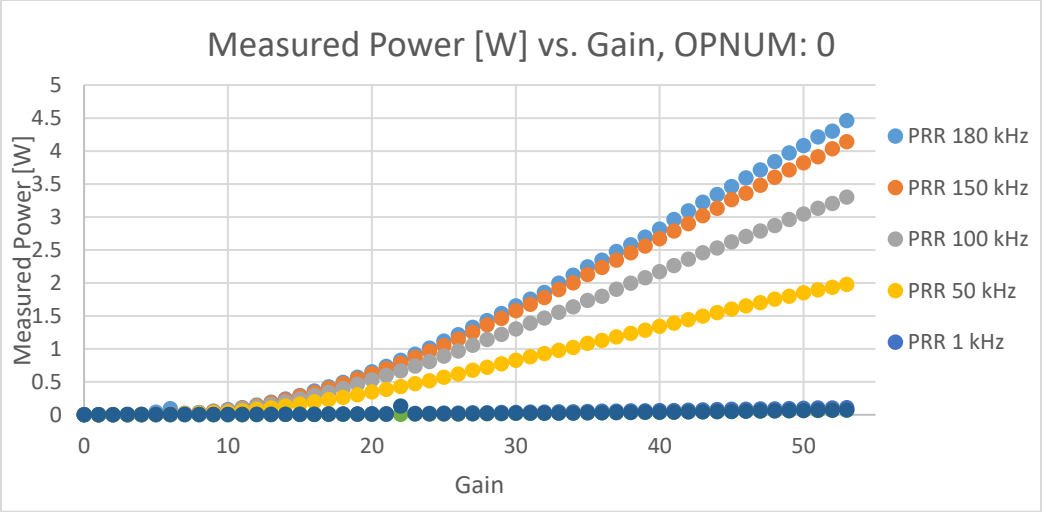

Figure 20. Measured power using OPNUM 0 setting for increasing gain at varying repetition rate

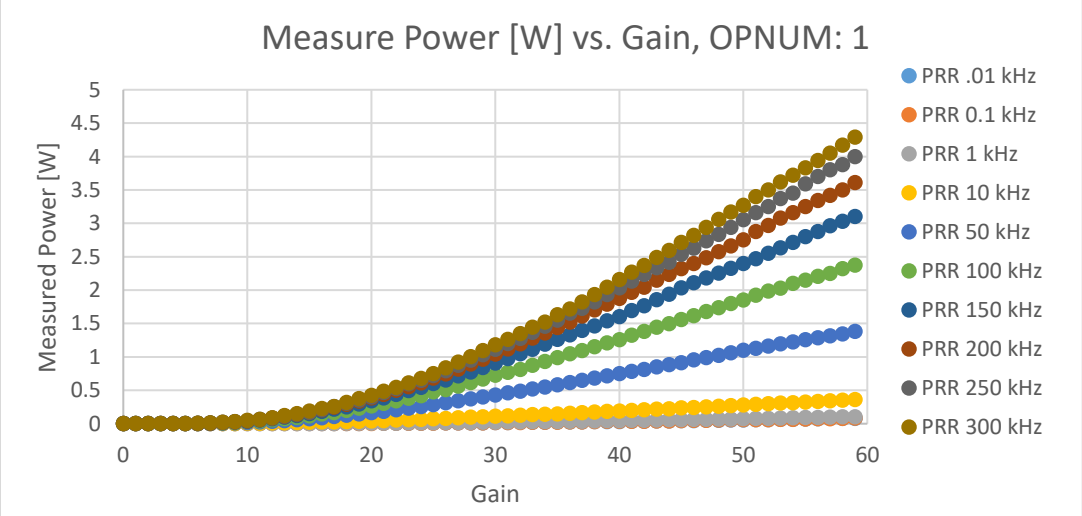

Figure 21. Measured power using OPNUM 1 setting for increasing gain at varying repetition rate

The theoretical average power and maximum power densities were calculated and organized to compared with the measured average power and maximum power densities in Table 4.

Table 4. Comparison of OPNUM 0 and 1 theoretical and measured power and power density

OPNUM	**0**	**1**
Max Theoretical Power [W]	10	10
Max Measured Power [W]	4.46	4.29
Max Theoretical Power Density [W/cm²]	1.93E+05	1.93E+05
Max Measured Power Density [W/cm²]	8.59E+04	8.27E+04
Theoretical Peak Power [W]	18333.3	11000
Th. Peak Power Density [W/cm²]	3.53E+08	2.12E+08
Measured Max Peak Power Density [W/cm²]	1.59E+08	9.19E+07

The maximum measured power values when the VGEN laser was initially received was surprisingly low as it was less than half of what the power should be according to the specification. However, since the power densities calculated were deemed "enough" for the beam to be doubled in a BBO crystal, experiments were continued to double the beam to 532 nm and 266 nm.

As of the week of December 12, 2016, the power output of the laser decreased drastically to the point where power measurements could not be distinguished from noise. As a result, the laser was sent back to Spectra Physics for repair. The laser was returned on February 17, 2017 with software updates, and the measured power now reflects the specifications given from Spectra Physics. The measured data and graphs can be seen in Appendix A.

3.2 Doubling the Laser and using a BBO Crystal

One unexpected challenge we faced was frequency doubling the 532 nm laser into the 532 nm and 266 nm beams. The concept of frequency doubling, also known as second harmonic generation (SHG) is

when an input wave is converted into another wave with twice the frequency of the input wave in the medium. A medium that doubles the optical frequency typically occurs in crystal materials that lack inversion symmetry as they exhibit a $\chi^{(2)}$ nonlinearity [43]. This $\chi^{(2)}$ nonlinearity generates a nonlinear polarization wave that oscillates with double the fundamental frequency and also radiates an electromagnetic field with the doubled frequency. This generated second-harmonic field propagates predominantly in the direction of the nonlinear polarization wave.

For our application, we have a 532 nm Nd:YAG pulsed fiber laser that is to be doubled into 532 nm and 266 nm. The crystal that was ordered is a BBO type 1 for 532 nm second harmonic generation from United Crystals (65 Linwood Road North, Port Washington, NY 11050-1439). Unfortunately, the maximum power output of the laser at the time when it was first received made doubling not possible to achieve. Discussions with the United Crystal representative suggested that the power density of a fiber laser was not enough for SHG, as the Q-switched lasers seemed to be more appropriate for the purchased BBO. Another BBO crystal from EKSMA (Mokslininkų str. 11, LT-08412 Vilnius, Lithuania) was also bought to narrow down whether the trouble with doubling was because of the BBO crystal itself or if it was from the laser. UV light could not be achieved with the use of this second crystal, thus hinting that the output power of the laser was not enough for second harmonic generation to occur in the BBO crystal. Efforts to double were continued when the laser was repaired and returned. As of the February 27, 2017, 10 days after the return of the laser, 266 nm light was achieved through both the BBO crystal from United Crystals and the BBO crystal from EKSMA.

3.3 Beam Size Measurement at the Sample Position

The beam size at the sample plane was measured in the x and y direction using the knife-edge test and a power meter. A blade was mounted onto a 3-axis linear stage with a precision of 10 micron increments, where the beam would be blocked in either the x or y direction for different z heights. The height of the knife was varied to find the height of the smallest spot size. The x and y directions were measured because

the beam at the sample plane is elliptical due to the angle between the principle beam axis and the sample plane. Figure 22 shows an image of the setup without the power detector and Figure 23 gives a top-down view of the entire setup with the power detector.

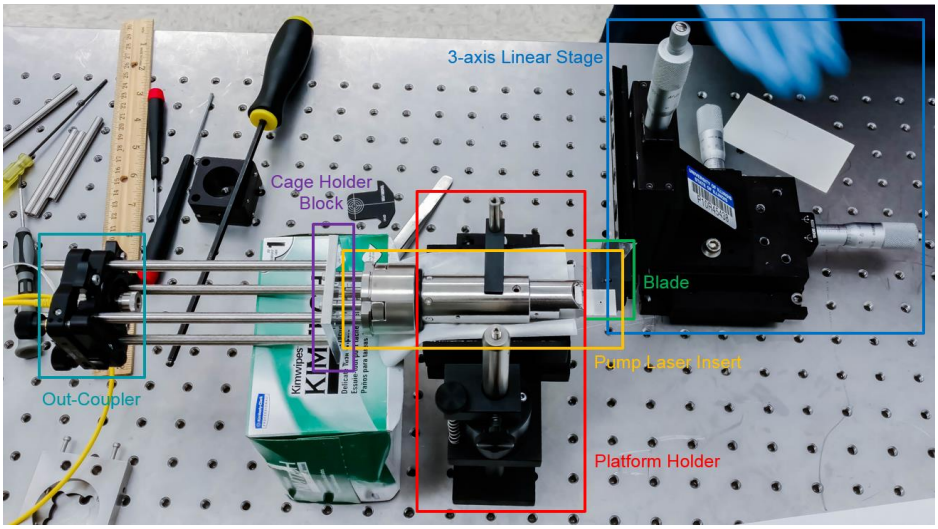

Figure 22. Labeled image of general setup to measure beam size at the sample plane. From the left-most box is the out-coupler of a single-mode fiber (teal), cage holder block (purple), pump laser insert (yellow), platform holder (red), razor blade (green), and 3-axis linear stage (blue).

Since a detector is placed on the optical table for measuring the power, the diverging beam after the focal point at the plane of the beam alignment plate is too large for the detector. A lens was placed to focus the diverging beam onto a detector. The measured values were the recorded power of a fully blocked beam to a fully unblocked beam, or vice versa.

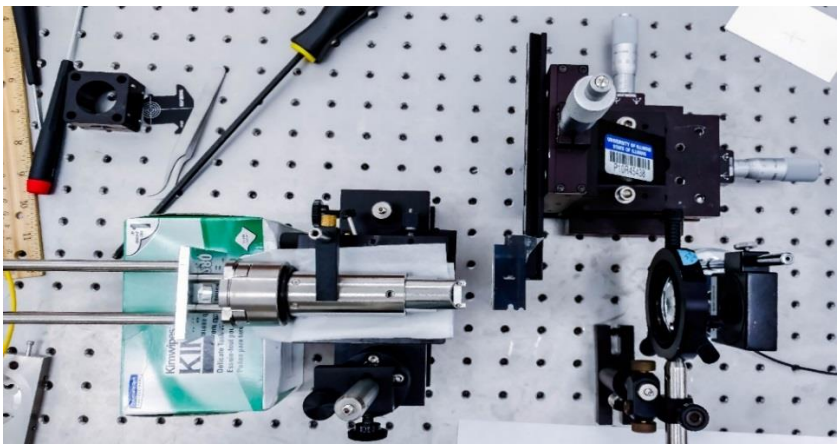

Figure 23. Top-down view of beam measurement setup with power detector, where the magnifying glass placed before the power detector focuses the expanding beam into the power detector for better power measurement.

To find the focal point, the Foucault knife-edge test [44] can be implemented. By moving the blade on the translation stage and looking for the focal plane, a shadow of a half-circle will appear when the knife-edge is not at the focus and a uniform shadow will appear when the blade is at the focal plane. Alternatively, the hole in the beam alignment plate indicates the location of the focal point from the Pump Laser Insert.

The locations and respective power readings for minimum (fully blocked beam) to maximum (fully unblocked beam) were noted during the measurement period. Measurements were recorded in increments of 10 μm until readings hit its maximum or minimum. The power measurements can be plotted (Figure 24) and fitted using Equation 5 to calculate the beam width. Two types of calculations are made: 10-90 and FWHM. The 10-90 calculation is the difference of the power measurements at 10% and 90% of its maximum measured power, and the full width at half maximum is the derivative of the initial measurements to find the difference of the values at half of the maximum value.

$$y = y_0 + \frac{A}{2}\left[Erf\left(\frac{2\sqrt{ln2}}{FWHM}(x - x_c)\right) + 1\right] \quad \text{(Equation 5)}$$

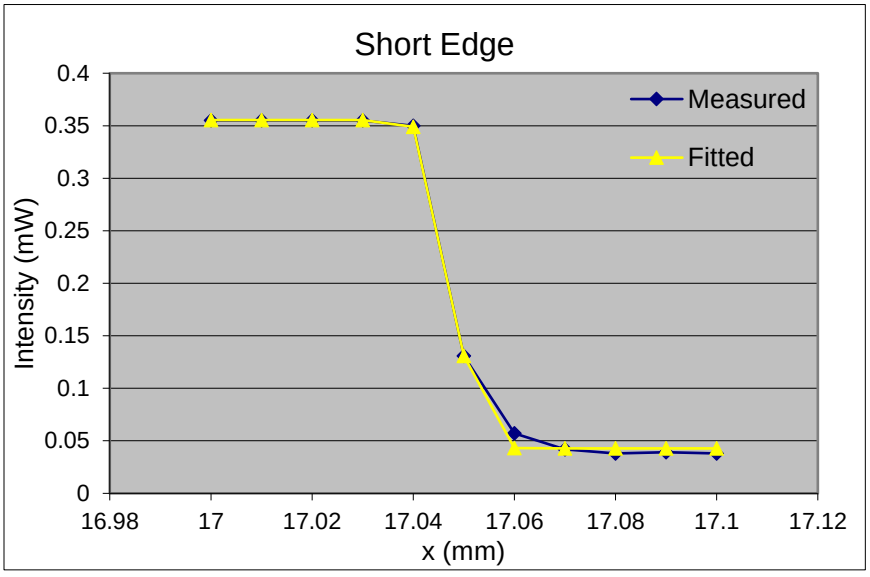

Figure 24. Measured and fitted intensity of beam at focal point

With various z heights and repeated measurements, it was determined that the smallest spot size obtained for both short and long edge of the beam averaged at 9.48 μm and 47.26 μm respectively. With these values, the smallest spot size on the focal plane at the plane perpendicular to the light propagation direction can be calculated knowing the angle of incidence.

3.4 Theoretical Pump-Probe Overlap in the TEM

The overlap of the pump delivery system (laser beam) and the electron beam was calculated very simply to estimate how much time passes when the two beams overlap over the sample, defining time zero as when the overlap begins. A schematic can be found in Figure 25.

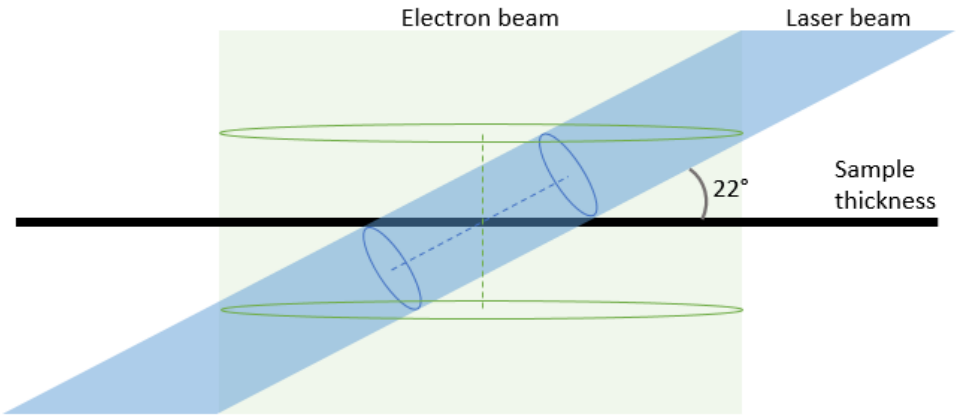

Figure 25. Labeled schematic of pump and probe overlap. The outlined circles for both beams indicate the area of overlap over the sample.

Assuming a sample thickness of 100 nm, the distance of electron beam and laser beam crossing over the sample and overlapping each other were calculated to be 32.92 μm and 44.08 μm respectively. Using the simplified equation for rate (Equation 6), a rough estimate of the time of overlap can be determined.

$$t = \frac{D}{c} \qquad \text{(Equation 6)}$$

Where c_{light} = 2.998 x 10^8 m/s and $c_{electron}$ = 2.328 x 10^8 m/s. The time for laser and electron beam would be as follows:

Laser:

$$t = \frac{D}{c_{light}} = \frac{44.08\mu m}{2.998\ x\ 10^8\ m/s}$$

$$t = 147\ fs$$

Electron beam:

$$t = \frac{D}{c_{electron}} = \frac{32.92\mu m}{2.328\ x\ 10^8\ m/s}$$

$$t = 141.4\ fs$$

3.5 Communication between BNC Digital Delay Generator and VGEN Laser

Operation of the laser is aimed to be controlled by a Digital Delay Generator (DDG) from Berkeley Nucleonics Corporation (BNC) [45]. The Model 577 Pulse Generator is used to control the pulse characteristics and behavior, which can also be programmed using the LabView software. An oscilloscope was used to observe the pulses being outputted from the DDG and to find the settings of the DDG to match the pulses from the function generator, where the function generator simulates the pulses desired from the laser. The schematic of how the instruments were connected and to which ports are detailed in Figure 26.

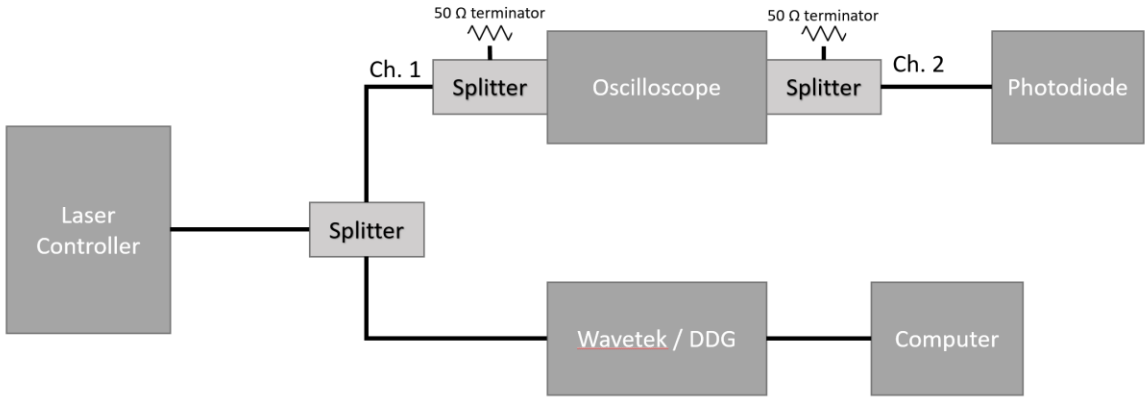

Figure 26. Schematic of the connections and instruments used to visualize the pulses acting as triggers from the Wavetek or Berkeley Nucleonics Corporation digital delay generator and the pulses being emitted by the laser controller..

While the laser can arm and fire using an RS232 signal, the goal of the overall setup is to use the DDG as the external trigger for the laser to generate a sequence of pulses defined by the pulse generator. The user can define a variety of pulse sequences with the pulse generator itself or its accompanying LabView software. However, the signal from the delay generator to the laser controller is a TTL signal, therefore needing the use of the TTL D25 connector of the laser controller. The D25 connector is also utilized as a safety of the laser controller, requiring two pins (15 & 23) to be connected (shorted) for the laser to function for arm and fire. Because individual efforts for communicating the DDG to the laser controller were not fruitful and personal knowledge was insufficient to efficiently move the project forward, this part of the project was in collaboration with MRL staff Lon Westfall.

To establish communication between the DDG and the laser with a TTL signal, the D25 connector is manipulated so communication can take place. While the purpose of each pin in the D25 connector is elaborated in the VGEN manual (see Appendix B), the schematic of the D25 connector pins and how the pins are connected and used are illustrated in Figure 27 and Figure 28. An electrical schematic of the connections are illustrated in Appendix B.

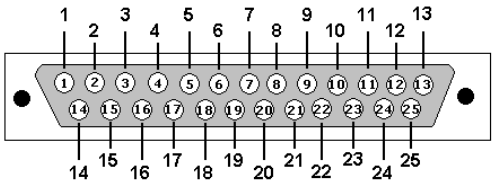

Figure 27. Schematic diagram of pin numbering used for D25 connector.

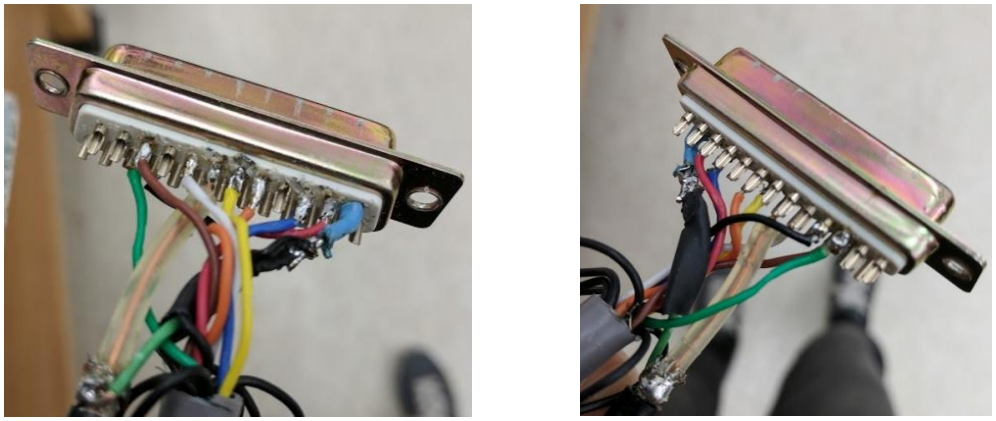

Figure 28. Image of D25 cable with pin connections exposed.

A switch was used to fire the laser with a TTL signal, where the center pin of the switch (PIN 19, laser active) connects to ground (PIN 10 & 14) for off, and connects to 5V (PIN 15) for fire. With this setup, TTL operation is possible with the VGEN software running in the background, where the TTL signal is specified and the laser is able to "ARM" and the switch is able to "FIRE" the laser when switched to "ON". Initially, the laser was unable to detect the external trigger provided by the delay generator, resulting in mismatching pulses between the delay generator and the laser. This mismatch comes from the setting on the VGEN software that initially specified that the trigger signal is "internal". This setting was switched to "external". However, pulses were not detected initially when the laser is set to "FIRE". This, we suspected, was due to the lack of external trigger detected by the laser from the delay generator. In discussion with the VGEN engineer, the VGEN software should detect a change in the pulse repetition rate from the delay generator and reflect the change in the software. A number of configurations were tested. By chance, with a Wavetek 5MHz Lin/Log Sweep Generator Model 185 [46], laser pulses were seen to be triggered by the pulse emitted from the Wavetek, with a period of 1 ms (1.00 kHz) and a peak to peak signal reading of 4.80V.

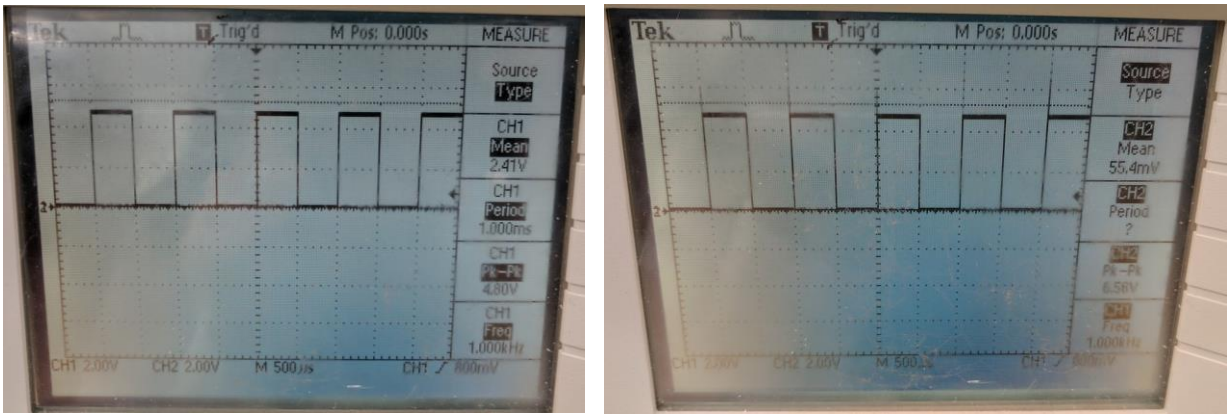

Figure 29. Signal from Wavetek, with a frequency of 1 kHz and pulse width of 500 µs (left) and with the pulses emitted from the laser controller (right).

The square signal in left image of Figure 29 is the signal from the Wavetek, and the small pulse peaks at the rising edge of the square signal in the right image of Figure 29 is the signal from the laser.

When the timing of the rising edge and the laser pulse is observed more closely, a delay of about 6 μs can be seen between the rising edge and the laser pulse, visible in Figure 30.

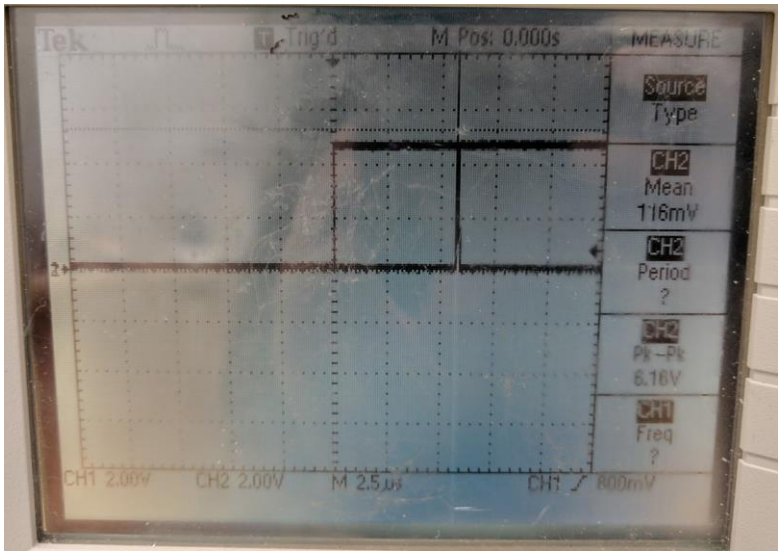

Figure 30. A single pulse from the laser controller and the Wavetek, showing the delay of the laser pulse to be about 6 μs after the rising edge of the Wavetek pulse.

Next, the same settings of 1 kHz repetition rate and pulse widths of 500 μs were configured on the BNC digital delay generator (DDG) LabView program, connecting the DDG to the laser in place of the Wavetek. Between changes in the conditions of the delay generator, the laser would be "OFF", meaning that the laser is not in "FIRE" not "ARM" mode. The settings of the LabView changed were the "Sys Period" (period) and "Chan. Width" (pulse length) before "running" the program to send the new commands to the DDG. This setup was successful with the DDG triggering laser pulses. This procedure was then followed for periods of 1 ms, 100 μs, 10 μs, and 5.6 μs for decreasing pulse widths, resulting in a variety of duty cycles being used to see if any of the conditions would "break" the triggering response being observed. For all conditions tested, recorded in Appendix C, the DDG served as an accepted trigger for the laser to fire a corresponding pulse.

3.6 Single-Shot Operation and Ex-Situ Testing with Quantifoil

Single-shot operation is possible with the BNC DDG LabView program by changing the "Sys Mode" from "Normal" to "Single", evident in Figure 31. By doing so, a single pulse can be seen on the oscilloscope over a time frame where there would normally be multiple pulses with continuous pulses.

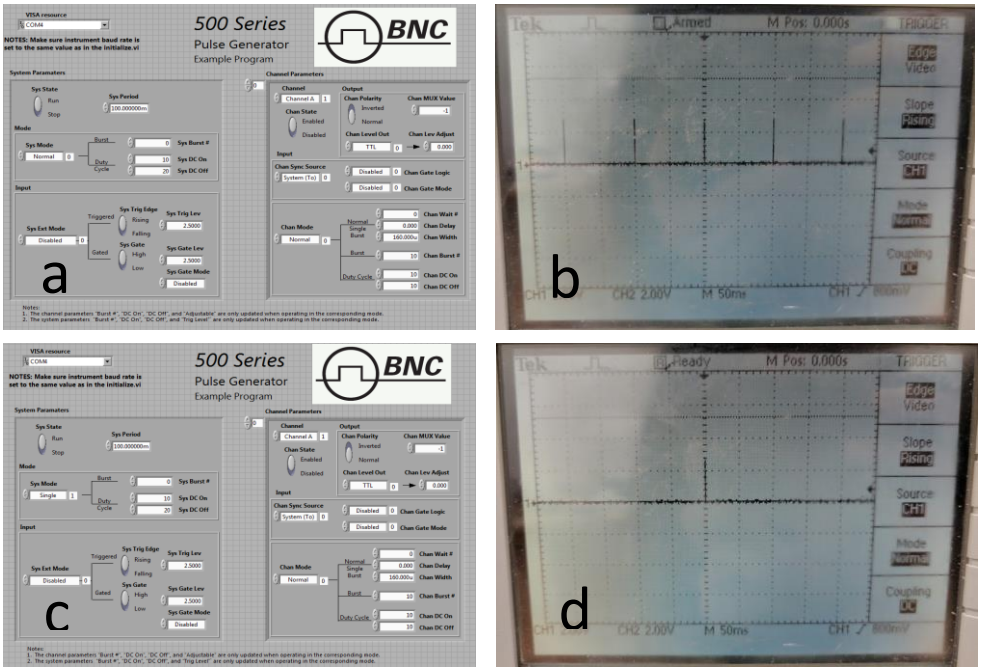

Figure 31. (a) BNC DDG LabView program settings for continuous trigger at a period of 100 ms and pulse widths of 160 µs and (b) visualization of the pulses sent by the BNC DDG on the oscilloscope. (c) BNC DDG LabView program settings for single trigger at a period of 100 ms and pulse width of 160 µs and (d) visualization of the pulse sent by the BNC DDG on the oscilloscope.

The laser pulse triggered by the DDG signal can be detected in a smaller time frame so that the DDG pulse can be seen to trigger the laser pulse, seen in Figure 32. With these two modes of laser triggering, the continuous trigger mode can be used to also measure the power of the laser beam and its respective gain, and the single trigger mode can be used for single-shot experiments onto the sample.

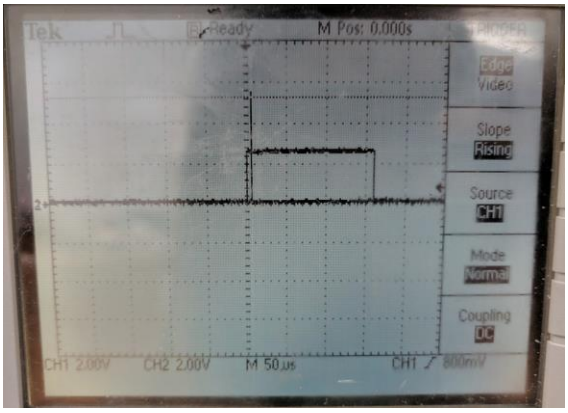

Figure 32. Single-shot of DDG trigger and laser pulse visualized onto oscilloscope.

The Quantifoil [47] setup is used to find the overlap between laser and electron beam inside the Hitachi H-9500. The Quantifoil is a 3mm diameter TEM grid that leaves a burn mark with high enough energies incident upon the grid. Given high enough energies it is possible for the grid to burn completely. The ex-situ experiments will aid in finding the minimum and maximum power limits that the Quantifoil can handle without destroying the polymer substrate. With this, the evidence of a single shot pulse can be seen externally on a TEM grid, and will act as a reference for when the experiment is repeated in the Hitachi H-9500, since the burn mark left behind will indicate the location and the center of the laser beam.

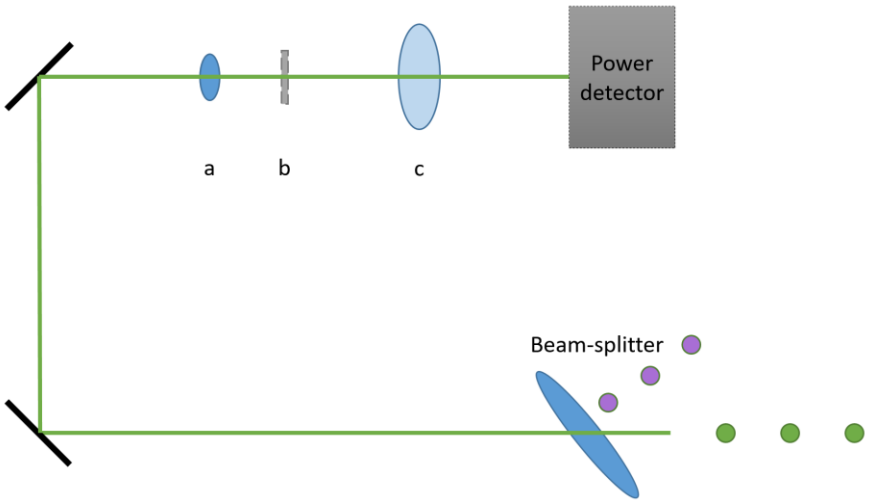

Figure 33. Setup for the ex-situ Quantifoil configuration. The green line is the 532 nm beam and the optical axis that passes through optics to simulate conditions of the pump delivery system in the Hitachi H-9500 and other instruments to measure the beam size, power, and its behavior. The green and purple dots are the 532 nm and 266 nm beams, respectively, and the corresponding optics that are not related to the quantifoil experiment explicitly. The optics directly related are (a) 6 mm diameter plano-convex lens with a focal length of 15 mm and about 20 nm of ITO coating (Thorlabs #LA 1222-A), (b) a blade used to conduct knife-edge tests for beam size, and also the plane in which the quantifoil was placed for single-shot experiments, and (c) a large lens to re-focus the diverging beam after the focal length of lens (a).

The setup, drawn out in Figure 33, consists of the additional optics (Figure 33a, b, c) being placed after the 532 nm beam undergoes second harmonic generation from the BBO crystal (EKSMA #BB0-700) and the 266 nm beam being deflected by the beam splitter (Thorlabs #HBSY13) in order to measure the beam size, power, and the behavior of the beam. The beam should be collimated (ideally as close to the 532 nm fiber cable being used to best simulate conditions of the pump delivery system in the Hitachi H-9500) before the 6 mm diameter lens (Thorlabs #LA1222-A). A knife blade is placed at the focal point of the 6 mm lens (f = 15 mm) with the assistance of a 3-axis stage to measure and record the beam size at the focal point using the knife-edge method. At some distance down the optical axis, the power of the beam is measured and recorded using a power detector and power meter (Astral AD30) with the help of a lens to re-focus the diverging beam after the 6 mm diameter lens. Additionally, to double check and make sure that a single shot pulse is being outputted by the laser, a photodiode connected to an oscilloscope can be placed before the entire setup to visually see the single shot pulse and confirm that triggering is occurring via oscilloscope. However, the photodiode must be removed to complete the single shot to ensure that the beam is not blocked by the photodiode. When all these checks are completed, the Quantifoil (Ted Pella, Inc #657-300-Cu) is placed on the blade edge via double-sided tape and the single shot should be run. The Quantifoil is then observed under an optical microscope for evidence of laser damage, with an image taken for recording purposes.

Preliminary testing of the single-shot Quantifoil experiment was conducted to visualize the laser damage onto a Quantifoil. More experiments are to be conducted after the completion of this thesis, since they were not able to be conducted in the given time frame. The laser beam was first measured using the knife-edge experiment, in the same fashion that the beam was measured at its focal point of the pump delivery system. After two rounds of measuring the beam (no beam to full beam to no beam), the full-width-half-maximum was calculated and averaged (Table 5) to a spot size of 71.82 μm.

Table 5. Full width at half maximum values for focused beam in Quantifoil singl-shot setup

	FWHM (mm)
Test 1	0.071737152
Test 2	0.071956668
Test 3	0.070764049
Test 4	0.072805649
Average	0.071815879

The Quantifoil experiment was continued even though the measured spot size is much larger than the expected beam size at the focal point of around 5 μm. The power of the laser at increasing gain was measured with continuous DDG trigger to record the power that would be released for a single-shot. For each gain value recorded, a single-shot was performed on a Quantifoil and placed into a specific slot in the Quantifoil holder for imaging afterward, organized into Table 6. The settings of the laser and the DDG were: laser power at 25%, repetition rate at 10 kHz, and the DDG trigger pulse width of 10 μs. These conditions were unchanged throughout this entire process. A Quantifoil grid with no laser damage was also imaged and placed in Slot 19A where all of the Quantifoil grids were stored as a control grid. For uniformity and ease of finding the laser mark, the Quantifoil grids were placed so that the laser beam was as close to the center of the grid as possible when the laser is armed so that the continuous wave light is visible but no pulses are being emitted.

Table 6. Power measurements of increasing gain and its corresponding power density and slot organization

Slot	Gain	Power (mW)	Power Density (W/cm²)
18A	20	35	8.64E+02
18B	25	62.5	1.54E+03
17A	30	89.6	2.21E+03
17B	35	123.5	3.05E+03
17C	40	159.5	3.94E+03
16A	45	198.5	4.90E+03
16B	50	220	5.43E+03
15A	55	254	6.27E+03
15B	60	286	7.06E+03

An Amscope (#MU300) 3MP USB 2.0 Microscope Digital Camera and its corresponding imaging software was used to capture images of the Quantifoil grids after performing the single-shot experiment.

From the micrographs obtained in Figure 34 at higher gains, there is quite clear evidence that the destroyed Quantifoil areas were a result of the laser single-shot pulse as opposed to some extraneous artifact of the Quantifoil grids prior to the single-shot experiment.

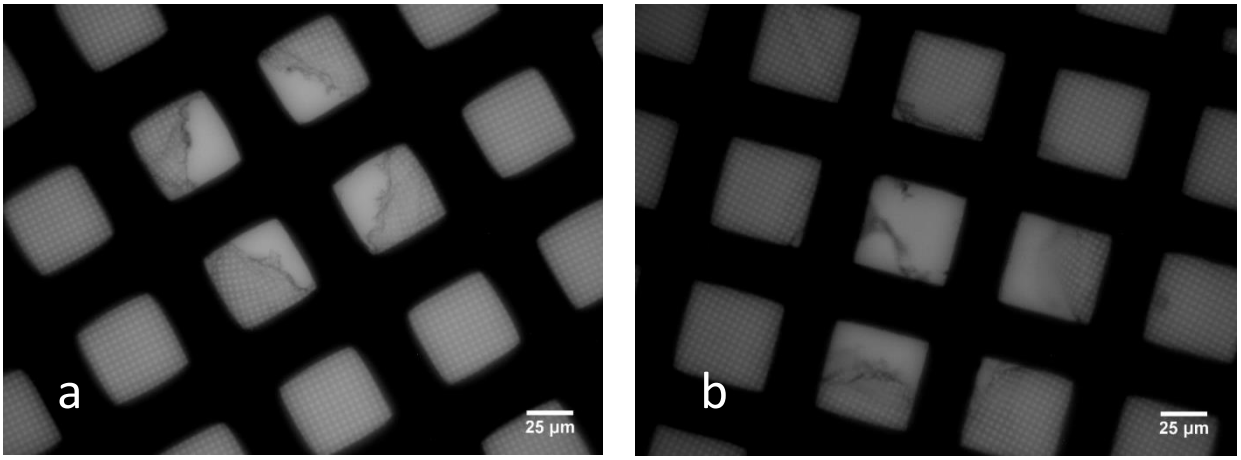

Figure 34. Micrographs of Quantifoil grids at 40X magnification after performing the single-shot experiment where (a) was shot with a gain of 45 and (b) was shot with a gain of 50.

For the smaller gain values (<35), there was no clear indication that any specific artifact found on the Quantifoil grid could be attributed to the laser single-shot. For most of the grids, many images of artifacts were under the assumption that the artifacts were not present prior to the single-shot experiment. Furthermore, because the spot size of the beam at the plane of the Quantifoil was larger than the spacing between the copper grids, it is possible that the energy of the beam was absorbed into the copper grids so that no mark was shown on the polymer substrate of the Quantifoil. One grid, shown in Figure 35, shows an artifact that has high potential of a laser burn mark at a gain of 35.

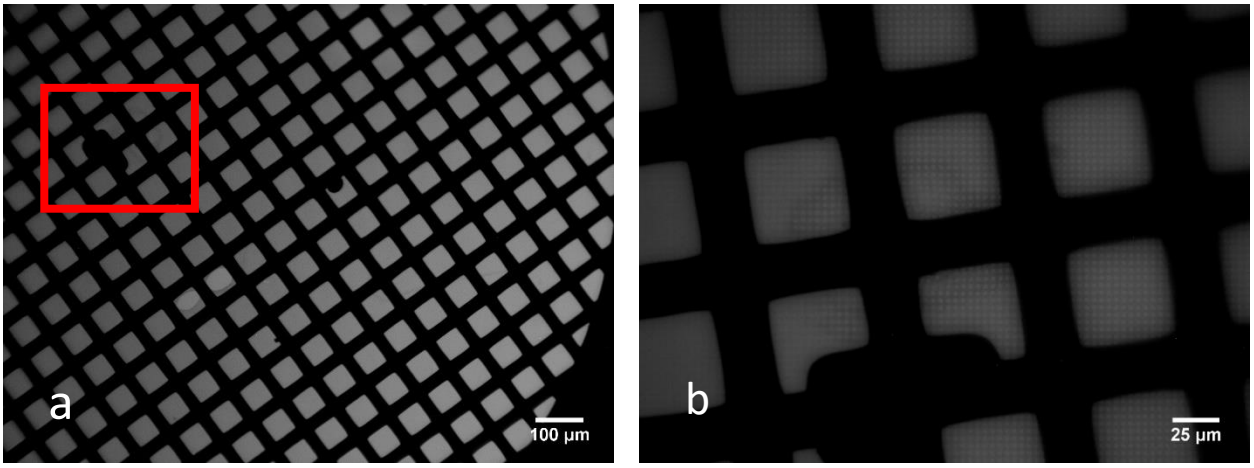

Figure 35. Quantifoil exposed to a gain of 35 for single-shot experiment with a mark that looks similar to a burn mark at (a) 10X magnification, with a red box marking the location of the burn mark, and (b) 40X magnification.

After the completion of this initial experimentation of the Quantifoil single-shot experiment, we observed that some Quantifoil grids contained defects. This experiment can be improved by imaging each Quantifoil grid prior to conducting a single-shot onto the grid. By having images of the Quantifoil grids used for the single-shot experiment, the images can be compared before and after the single-shot experiment to isolate out any artifacts that may have existed on the grid prior to the single-shot experiment. Then the artifacts created by laser damage can be identified more easily as the marks besides the ones that pre-existed on the Quantifoil grid. Alternatively, a line of single-shots can be made across a grid, thus making a pattern on the grid that can be easily detected under direct observation of an optical microscope.

CHAPTER 4

CONCLUSION AND OUTLOOK

This concludes the documentation of the dynamic environmental transmission electron microscope (DETEM) development efforts up to May 2017 at the University of Illinois Urbana Champaign. The Hitachi H-9500 300 kV TEM installed at the Frederick Seitz Materials Research Laboratory has the pump delivery system and cathode delivery system components installed in the sample stage and the extended column segment near the cathode of the TEM, both of them aligned appropriately prior to installation. Manuals on the assembly and alignment of both the pump delivery system and the cathode delivery system have been created for documentation purposes. The VGEN nanosecond pulsed fiber laser system has been characterized both before and after its repair to verify its power settings and understanding the behavior of the laser at a variety of settings in combination with multiple arrangements of optics to optimize the optical table setup. Laser doubling was achieved through both BBO crystals purchased upon the return of the repaired laser. Communication between the VGEN laser and the BNC pulse generator was established, allowing the DDG to trigger pulses from the VGEN laser. Single-shot settings and experiments were carried out on a Quantifoil in search of the power threshold for a burn mark to appear.

Looking ahead, there are still Quantifoil single-shot experiments to be done with the minimum spot size at the focal length of the 6 mm diameter lens to find the minimum and maximum power density needed for a burn mark to appear on the Quantifoil. After that, the optical table setup would be in its last stages of getting the 532 nm and 266 nm beams coupled into their respective fibers before relocating the optical table to the basement where the Hitachi H-9500 300 kV TEM is housed in the Frederick Seitz Materials Research Laboratory. Quantifoil experiments will continue in the Hitachi H-9500 to locate both the laser and electron beam, adjusting the optical inserts accordingly for the two beams to overlap. Once that is complete, experimentation with materials of interest may begin with the newly implemented DETEM.

REFERENCES

[1] A. H. Zewail and J. M. Thomas, 4D Electron Microscopy: Imaging in Space and Time, Convent Garden, London: Imperial College Press, 2010.

[2] E. Muybridge, "The horse in motion, illus. by Muybridge. "Sallie Gardner," owned by Leland Stanford, running at a 1:40 gait over the Palo Also track, 18 June 1878: 2 frames showing diagram of foot movements," 19 June 1878. [Online]. Available: www.loc.gov/pictures/item/2007678037.

[3] H. Edgerton, "Iconic Images - Apple Drop," 1987. [Online]. Available: edgerton-digital-collections.org/galleries/iconic.

[4] H. Edgerton, "Iconic Images - Bullet through apple," 1964. [Online]. Available: edgerton-digital-collections.org/galleries/iconic.

[5] D. J. Flannigan and A. H. Zewail, "4D Electron Microscopy: Principles and Applications," *Accounts of Chemical Research,* vol. 45, no. 10, pp. 1828-1839, 2012.

[6] P. E. Batson, N. Dellby and O. L. Krivanek, "Sub-angstrom resolution using aberration corrected electron optics," *Nature,* vol. 418, pp. 617-620, 2002.

[7] S. Uhlemann and M. Haider, "Residual wave aberrations in the first spherical aberration corrected transmission electron microscope," *Ultramicroscopy,* vol. 72, pp. 109-119, 1998.

[8] M. Haider, S. Uhlemann, E. Schwan, H. Rose, K. Bernd and K. Urban, "Electron microscopy image enhanced," *Nature,* vol. 392, pp. 768-769, 1998.

[9] M. Haider, P. hartel, H. Muller, S. Uhlemann and J. Zach, "Information Transfer in a TEM Corrected for Spherical and Chromatic Aberration," *Microscopy and Microanalysis,* vol. 16, pp. 393-408, 2010.

[10] A. Rosenauer, F. F. Krawuse, K. Muller, M. Schowalter and T. Mehrtens, "Conventional Tranmission Electron Microscopy Imaging beyond the Diffraction and Information Limits," *Physical Review Letters,* vol. 113, p. 09101, 2014.

[11] E. A. Stach, "Real-time observations with electron microscopy," *MaterialsToday,* vol. 11, pp. 50-58, 2008.

[12] J. E. Evans, K. L. Jungjohann, N. D. Browning and I. Arslan, "Controlled Growth of Nanoparticles from Solution with in Situ Liquid Transmission Electron Microscopy," *Nano Letters,* vol. 11, no. 7, pp. 2809-2813, 2011.

[13] H. Zheng, J. Wang, J. Y. Huang, J. Wang, Z. Zhang and S. X. Mao, "Dynamic Process of Phase Transition from Wurtzite to Zinc Blende Structure in InAs Nanowires," *Nano Letters,* vol. 13, no. 12, pp. 6023-6027, 2013.

[14] Y. Suzuki, G. Cardone, D. Restrepo, P. D. Zavattieri, T. S. Baker and F. A. Tezcan, "Self-assembly of coherently dynamic, auxetic, two-dimensional protein crystals," *Nature,* vol. 533, pp. 369-373, 2016.

[15] L. Wang, Y. Lu, D. Kong, L. Xiao, X. Sha, J. Sun, Z. Zhang and X. Han, "Dynamic and atomic-scale understanding of the twin thickness effect on dislocation nucleation and propagation activities by in situ bending of Ni nanowires," *Acta Materialia,* vol. 90, pp. 194-203, 2015.

[16] J. Kacher, Q. Yu, C. Chisholm, C. Gammer and A. M. Minor, "In Situ TEM Nanomechanical Testing," in *Conference Proceedings of the Society for Experimental Mechanics Series*, 2016.

[17] V. A. Lobastov and R. Z. A. H. Srinivasan, "Four-dimensional ultrafast electron microscopy," *Proceedings of the National Academy of Sciences of the United States of America,* vol. 102, no. 20, pp. 7069-73, 2005.

[18] O. Bostanjoglo, R. Elschner, Z. Mao, T. Nink and M. Weingartner, "Nanosecond electron microscopes," *Ultramicroscopy,* vol. 81, pp. 141-147, 2000.

[19] A. Feist, N. Bach, N. Rubiano da Silva, T. Danz, M. Moller, K. E. Priebe, T. Domrose, J. G. Gatzmann, S. Rost, J. Schauss, S. Strauch, R. Bormann, M. Sivis, S. Schafer and C. Ropers, "Ultrafast transmission electon microscopy using a laser-driven field emitter: Femtosecond resolution with a high coherence electron beam," *Ultramicroscopy,* vol. 176, pp. 63-73, 2017.

[20] T. LaGrange, M. R. Armstrong, K. Boyden, C. G. Brown, G. H. Campbell, J. D. Colvin, W. J. DeHope, A. M. Frank, D. J. Gibson, F. V. Hartemann, J. S. Kim, W. E. King, B. J. Pyke, B. W. Reed, M. D. Shirk, R. M. Shuttlesworth, B. C. Stuart, B. R. Torralva and N. D. Browning, "Single-shot dynamic transmission electron microscopy," *Applied Physics Letters,* vol. 89, p. 044105, 2006.

[21] H. Dömer and O. Bostanjoglo, "High-speed transmission electron microscope," *Review of Scientific Instruments,* vol. 74, no. 10, pp. 4369-4372, 2003.

[22] N. D. Browning, G. H. Campbell, J. E. Evans, T. B. LaGrange, K. L. Jungjohann, J. S. Kim, D. J. Masiel and B. W. Reed, "Dynamic Transmission Electron Microscopy," in *Handbook of Nanoscopy*, 1 ed., G. Van tendeloo, D. Van Dyck and S. J. Pennycook, Eds., Weinheim, Wiley-VCH Verlag GmbH & Co. KGaA, 2012, pp. 309-343.

[23] T. LaGrange, B. W. Reed and D. J. Masiel, "Movie-mode dynamic electron microscopy," *MRS Bulletin,* vol. 40, no. 1, pp. 22-28, 2015.

[24] G. Khitrova, P. R. Berman and M. S. Iii, "Theory of pump-probe spectroscopy," *Optical Society of America,* vol. 5, no. 1, pp. 160-170, 1988.

[25] T. LaGrange, G. H. Campbell, B. W. Reed, M. Taheri, J. B. Pesavento, J. S. Kim and N. D. Browning, "Nanosecond time-resolved investigations using the in situ of dynamic transmission electron microscope (DTEM)," *Ultramicroscopy,* vol. 108, pp. 1441-1449, 2008.

[26] t. LaGrange, B. W. Reed, M. K. Santala, J. T. McKeown, A. Kulovits, J. M. K. Wiezorek, L. Nikolova, F. Rosei and B. J. Siwick, "Approaches for ultrafast imaging of transient materials processes in the transmission electron microscope," *Micron,* vol. 43, no. 11, pp. 1108-1120, 2012.

[27] G. H. Campbell, T. LaGrange, J. S. Kim, B. W. Reed and N. D. Browning, "Quantifying transient states in materials with the dynamic transmission electron microscope," *Electron Microscopy,* vol. 59, no. S1, pp. S67-S74, 2010.

[28] J. S. Kim, T. LaGrange, B. W. Reed, R. Knepper, T. P. Weihs, N. D. Browning and G. H. Campbell, "Direct characterization of phase transformations and morphologies in moving reaction zones in Al/Ni nanolaminates using dynamic transmission electron microscopy," *Acta Materialia,* vol. 59, no. 9, pp. 3571-3580, 2011.

[29] J. S. Kim, T. LaGrange, B. W. Reed, M. L. Taheri, M. R. Armstrong, W. E. King, N. D. Browning and G. H. Campbell, "Imaging of transient structures using nanosecond in situ TEM," *Science,* vol. 321, no. 5895, pp. 1472-1475, 2008.

[30] T. LaGrange, G. H. Campbell, P. E. A. Turchi and W. E. King, "Rapid phase transformation kinetics on a nanoscale: Studies of the $\alpha \rightarrow \beta$ transformation in pure, nanocrystalline Ti using the nanosecond dynamic transmission electron microscope," *Acta Materialia,* vol. 55, no. 15, pp. 5211-5224, 2007.

[31] T. LaGrange, D. S. Grummon, B. W. Reed, N. D. Browning, W. E. King and G. H. Campbell, "Strongly driven crystallization processes in a metallic glass," *Applied Physics Letters,* vol. 94, no. 18, p. 184101, 2009.

[32] L. Nikolova, T. LaGrange, B. W. Reed, M. J. Stern, N. D. Browning, G. H. Campbell, J.-C. Kieffer, B. J. Siwick and F. Rosei, "Nanocrystallization of amorphous germanium films observed with nanosecond temporal resolution," *Applied Physics Letters,* vol. 97, p. 203102, 2010.

[33] J. T. McKeown, A. K. Kulovits, C. Liu, K. Zweiacker, B. W. Reed, T. LaGrange, J. M. K. Wiezorek and G. H. Campbell, "In situ transmission electron microscopy of crystal growth-mode transitions during rapid solidification of a hypoeutectic Al–Cu alloy," *Acta Materialia,* vol. 65, pp. 56-68, 2014.

[34] M. L. Taheri, T. LaGrange, B. W. Reed, M. R. Armstrong, G. H. Campbell, W. J. DeHope, J. S. Kim, W. E. King, D. J. Masiel and N. D. Browning, "Laser-based in situ techniques: Novel methods for generating extreme conditions in TEM samples," *Microscopy Research & Technique,* vol. 72, no. 3, pp. 122-130, 2009.

[35] J. M. Zuo, R. Nuzzo, S. Dillon, X. Li and W. Wilson, "MRI: Development of a Dynamic Environmental Transmission Electron Microscope. Award Abstract #1229454," 2012. [Online]. Available: https://www.nsf.gov/awardsearch/showAward?AWD_ID=1229454&HistoricalAwards=false.

[36] Gatan, "Gatan K2 IS Camera Model 1010," 2015. [Online]. Available: http://www.gatan.com/products/tem-imaging-spectroscopy/k2-camera#resources.

[37] T. Kamino, "The function and benefits of a multifunctional heating holder developed for use with conventional high resolution analytical TEMs," in *Journal of Physics: Conference Series 126*, 2008.

[38] A. Yoon, W. Gao, J. Wu, H. Park, J. Mabon, W. L. Wilson and J.-M. Zuo, "Materials Processes Observed using Dynamical Environmental TEM at University of Illinois," *Microscopy and Microanalysis,* vol. 21, no. Suppl 3, pp. 2323-2324, 2015.

[39] "Transmission Electron Microscope H-9500," Hitcachi High Technologies Inc., 2006. [Online]. Available: http://www.hitachi-hightech.com/global/product_detail/?pn=em-h9500.

[40] Hitachi High-Technologies Corporation, "Instruction Manual for Model H-9500 Transmission Electron Microscope (User's Operation & Maintaenance, Ver.01.08 upward)," 2006.

[41] H. Park, *ProgressReports-1,* 2016.

[42] Spectra-Physics, "VPFL-G-10-HE User Guide," 2016.

[43] P. A. Franken, A. E. Hill, C. W. Peters and G. Weinreich, "Generation of Optical Harmonics," *Physical Review Letters,* vol. 7, no. 4, p. 118, 1961.

[44] G. Rodriguez, J. Villa, R. Ivanov, E. Gonzalez and G. Martinez, "Fouault test: a quantitative evaluation method," *Optical Society of America A,* vol. 33, no. 8, pp. 1604-1611, 2016.

[45] "Model 577 - Digital Delay / Pulse Generator," [Online]. Available: http://www.berkeleynucleonics.com/model-577.

[46] "Wavetek Microelectronics Corporation," [Online]. Available: http://www.wtkmicro.com/cht.cc/index.asp.

[47] "Quantifoil," [Online]. Available: http://www.quantifoil.com/.

APPENDIX A

UPDATED LASER POWER MEASUREMENTS

Power measurements when laser was returned fixed and with updates on February 17, 2017.

Measurements taken by Allan Sykes.

OPNUM 0, 150 kHz						
	Power					
Gain	0	20	40	60	80	100
20	0.23	0.28	0.35	0.43	0.56	0.72
30	0.78	0.94	1.14	1.40	1.75	2.22
35	1.14	1.38	1.64	2.00	2.51	3.11
40	1.52	1.83	2.20	2.67	3.29	4.10
45	1.96	2.33	2.80	3.37	4.15	5.10
50	2.40	2.86	3.40	4.14	4.97	6.13
60	3.30	3.92	4.63	5.61	6.65	7.97

OPNUM 0, 180 kHz						
	Power					
Gain	0	20	40	60	80	100
20	0.25	0.31	0.39	0.50	0.65	1.01
30	0.82	1.01	1.25	1.58	2.03	2.96
35	1.21	1.49	1.83	2.28	2.92	4.10
40	1.63	2.01	2.45	3.03	3.84	5.36
45	2.10	2.56	3.12	3.86	4.80	6.63
50	2.57	3.10	3.80	4.70	5.77	7.90
60	3.48	4.32	5.20	6.33	7.83	10.14

The following graph shows the power at different power settings, where a repetition rate of 150 kHz is graphed with a solid line and a repetition rate of 180 kHz is graphed with a dotted line for increasing gain values.

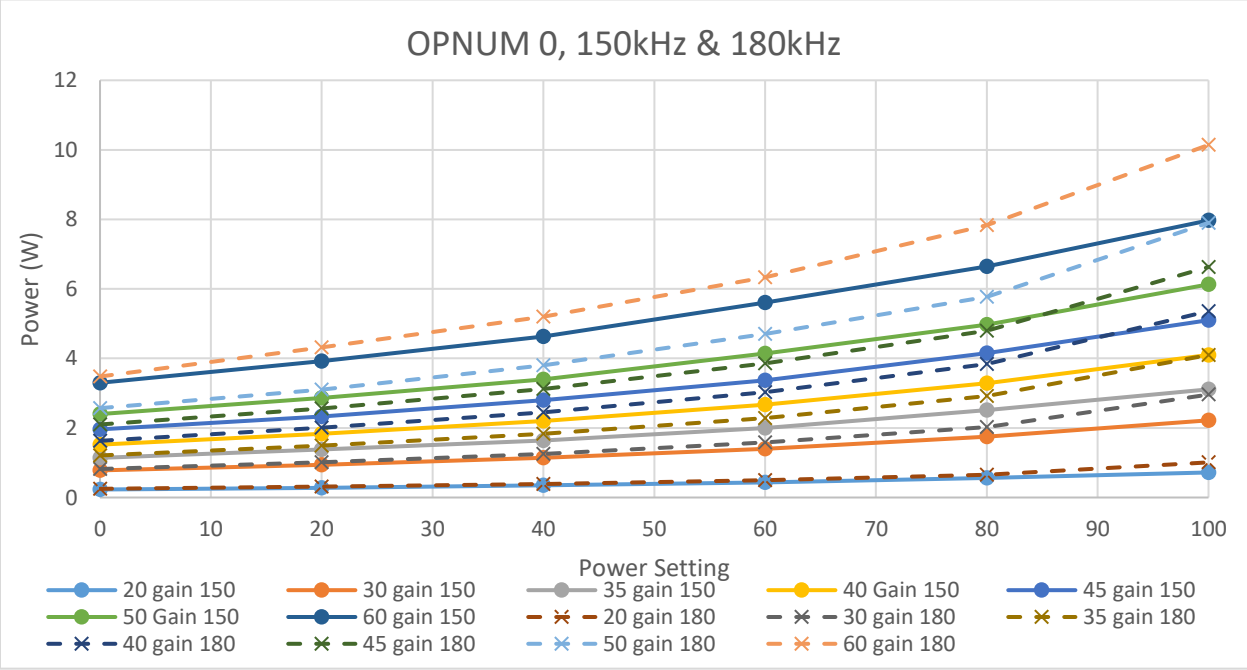

The following graph shows the power at different gain settings, where a repetition rate of 150 kHz is graphed with a solid line and a repetition rate of 180 kHz is graphed with a dotted line for increasing power values.

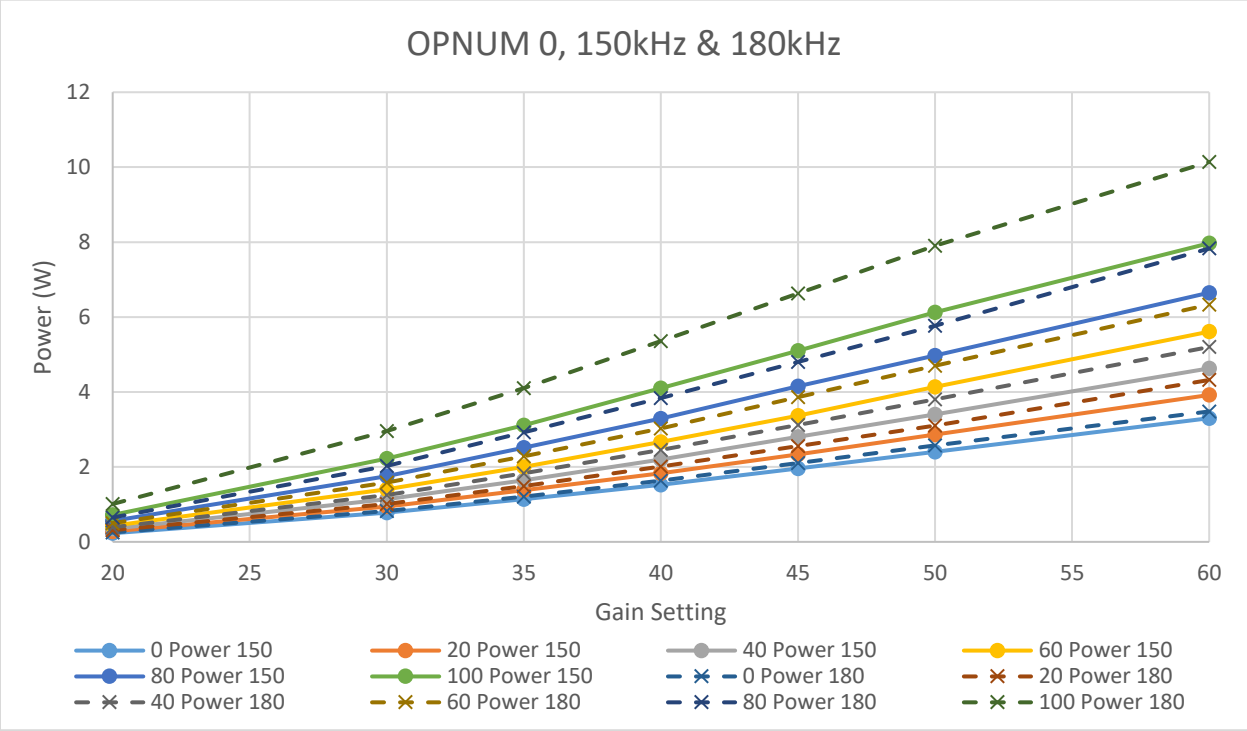

Power Density

OPNUM 0, 150 kHz						
	Power					
Gain	0	20	40	60	80	100
20	0.2	0.2	0.2	0.3	0.4	0.5
30	0.6	0.7	0.8	1.0	1.2	1.6
35	0.8	1.0	1.2	1.4	1.8	2.2
40	1.1	1.3	1.6	1.9	2.3	2.9
45	1.4	1.6	2.0	2.4	2.9	3.6
50	1.7	2.0	2.4	2.9	3.5	4.3
60	2.3	2.8	3.3	4.0	4.7	5.6

OPNUM 0, 180 kHz						
	Power					
Gain	0	20	40	60	80	100
20	0.1	0.2	0.2	0.3	0.4	0.6
30	0.5	0.6	0.7	0.9	1.2	1.7
35	0.7	0.9	1.1	1.3	1.7	2.4
40	1.0	1.2	1.4	1.8	2.3	3.2
45	1.2	1.5	1.8	2.3	2.8	3.9
50	1.5	1.8	2.2	2.8	3.4	4.7
60	2.1	2.5	3.1	3.7	4.6	6.0

The following graph shows the power at different power settings, where a repetition rate of 150 kHz is graphed with a solid line and a repetition rate of 180 kHz is graphed with a dotted line for increasing gain values.

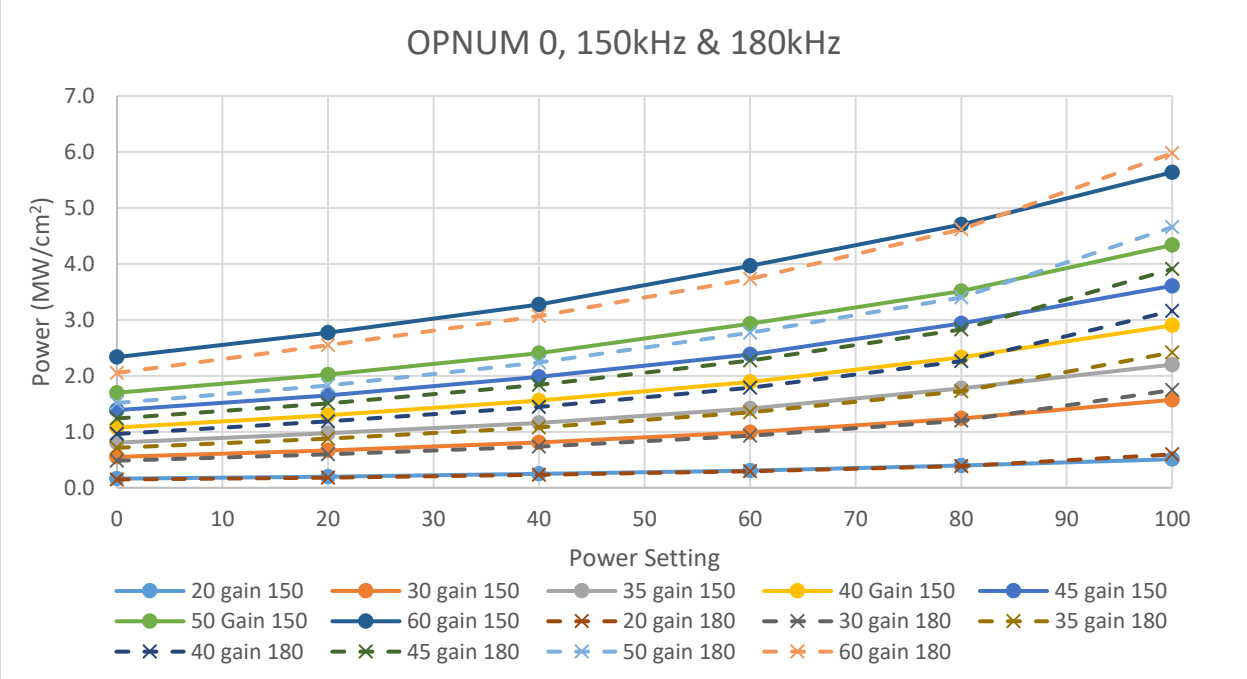

The following graph shows the power at different gain settings, where a repetition rate of 150 kHz is graphed with a solid line and a repetition rate of 180 kHz is graphed with a dotted line for increasing power values.

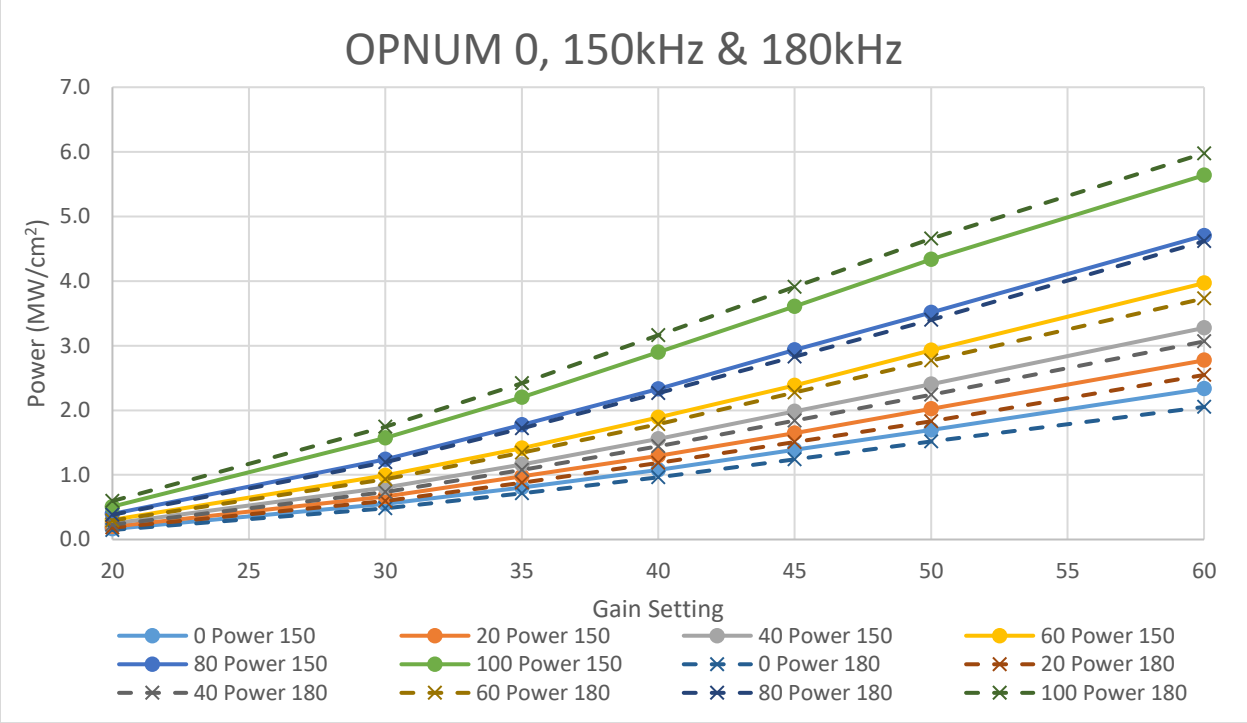

Pulse Energy

OPNUM 0, 150 kHz						
	Power					
Gain	0	20	40	60	80	100
20	1.5	1.9	2.3	2.9	3.7	4.8
30	5.2	6.3	7.6	9.3	11.7	14.8
35	7.6	9.2	10.9	13.3	16.7	20.7
40	10.1	12.2	14.7	17.8	21.9	27.3
45	13.1	15.5	18.7	22.5	27.7	34.0
50	16.0	19.1	22.7	27.6	33.1	40.9
60	22.0	26.1	30.9	37.4	44.3	53.1

OPNUM 0, 180 kHz						
	Power					
Gain	0	20	40	60	80	100
20	1.7	2.1	2.6	3.3	4.3	6.7
30	5.5	6.7	8.3	10.5	13.5	19.7
35	8.1	9.9	12.2	15.2	19.5	27.3
40	10.9	13.4	16.3	20.2	25.6	35.7
45	14.0	17.1	20.8	25.7	32.0	44.2
50	17.1	20.7	25.3	31.3	38.5	52.7
60	23.2	28.8	34.7	42.2	52.2	67.6

The following graph shows the power at different power settings, where a repetition rate of 150 kHz is graphed with a solid line and a repetition rate of 180 kHz is graphed with a dotted line for increasing gain values.

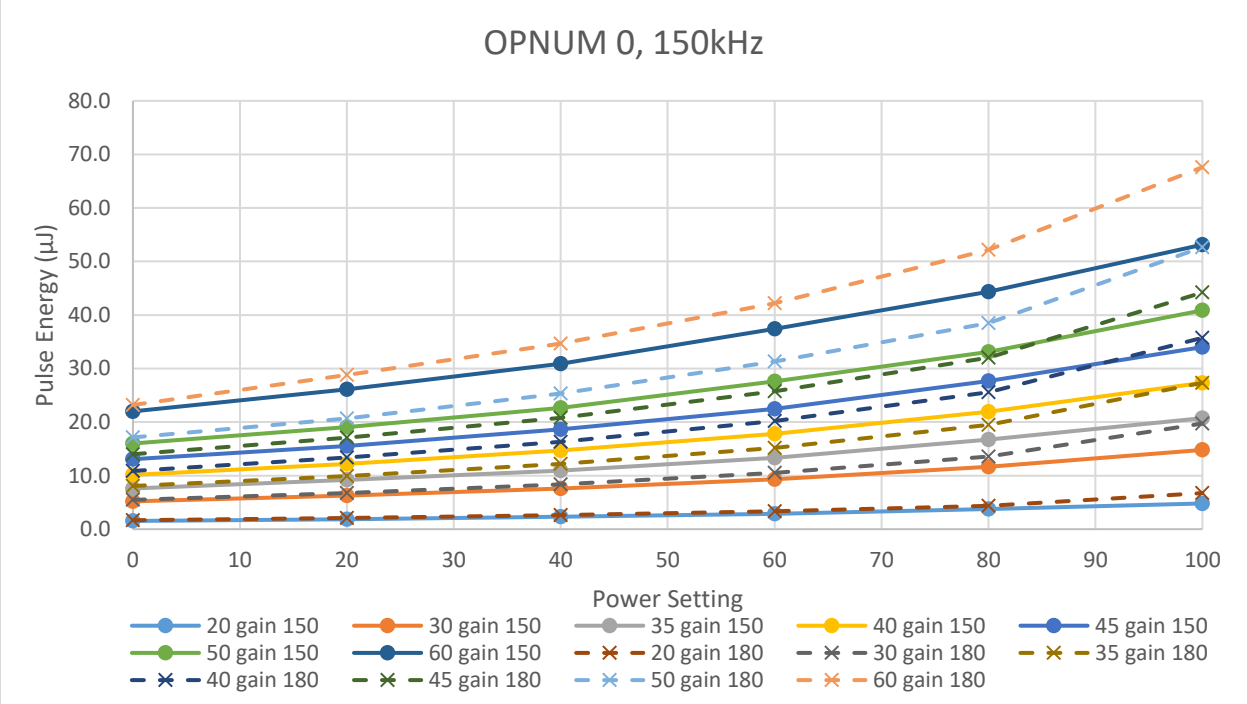

The following graph shows the power at different gain settings, where a repetition rate of 150 kHz is graphed with a solid line and a repetition rate of 180 kHz is graphed with a dotted line for increasing power values.

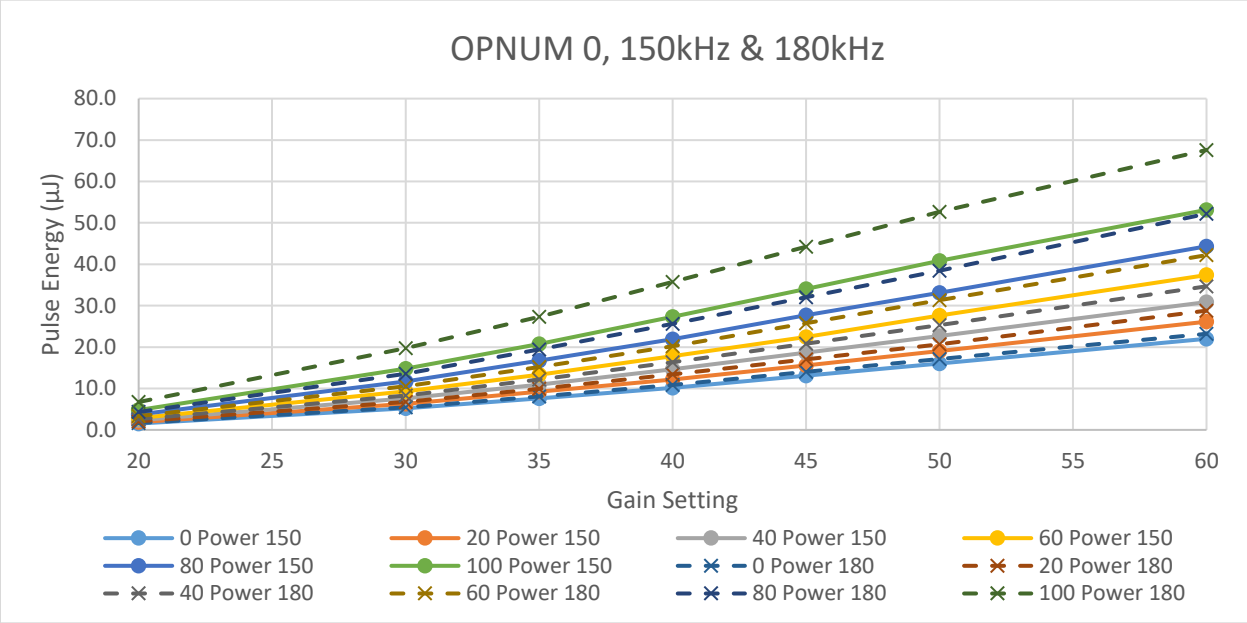

APPENDIX B

TTL SIGNAL D25

Table 7. D25 pin functions and remarks from VGEN User Manual

Pin	Name	Input/Output	Remarks
1	Power 0 LSB	I	8 bit TTL power
2	Power 1	I	8 bit TTL power
3	Power 2	I	8 bit TTL power
4	Power 3	I	8 bit TTL power
5	Power 4	I	8 bit TTL power
6	Power 5	I	8 bit TTL power
7	Power 6	I	8 bit TTL power
8	Power 7 MSB	I	8 bit TTL power (max power=11111111)
9	Latch	I	Latches power setting by rising edge of the signal
10	Modulation return		Return for laser modulation (pin19)
11, 16, 21	Laser alarms	O	Laser alarms status
12, 13, 17, 24, 25	Reserved		
14	Ground		
15	5V output	O	Utility power for users with 50mA max current
18	Laser Arm	I	Low emission when high
19	Laser Active	I	Full emission when high
20	PRR input	I	External laser PRR signal
22	Laser Guide	I	Currently not implemented
23	Emergency stop		HIGH: normal operation LOW: Stop

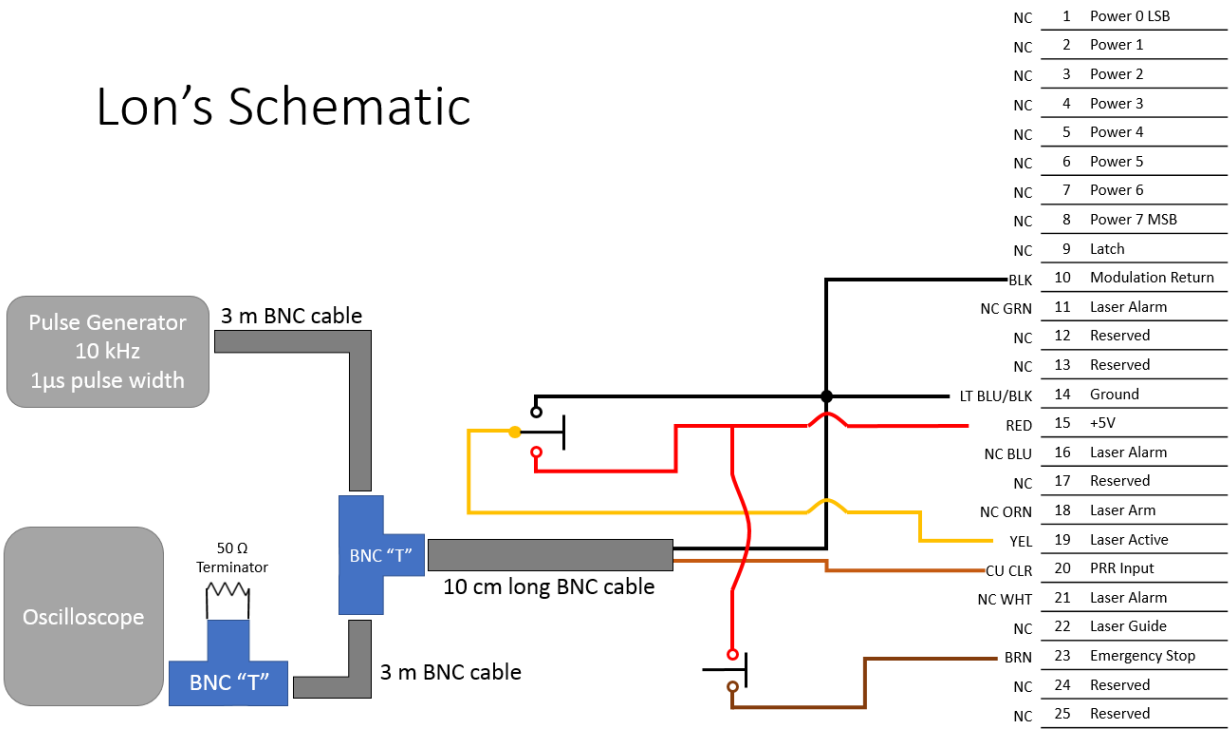

The above schematic was initially drawn by Lon Westfall, who is part of the Frederick Seitz Materials Research Laboratory staff, and digitally redrawn by Jocelyn Lai. This electrical schematic is of the D25 connector in relation to usage with the oscilloscope and the BNC DDG using TTL signal. All connections along with the construction of the D25 connector and cable were completed by Lon Westfall.

APPENDIX C

BNC DDG TRIGGER SETTINGS

Specific settings of the BNC digital delay generator, along with the corresponding readings on the VGEN GUI and confirmation of the pulses from the DDG and laser through the oscilloscope were recorded and images corresponding to most settings are also recorded in this Appendix.

OPNUM	**0**
Period	**1 ms**
Duty Cycle	***50%***

DDG	
Channel width	500 µs
Oscilloscope readings	
Period	1.00 ms
Frequency	1.00 kHz
Peak-Peak	2.72 V

VGEN GUI	
PRR	4.54 kHz

Photodiode	
Pulses seen?	Yes
In sync with signal rising edge?	Yes
~6 µs delay from rising edge?	Yes

Duty Cycle	***25%***

DDG	
Channel width	250 µs
Oscilloscope readings	
Period	1.00 ms
Frequency	1.00 kHz
Peak-Peak	2.72 V

VGEN GUI	
PRR	4.54 kHz

Photodiode	
Pulses seen?	Yes
In sync with signal rising edge?	Yes
~6 µs delay from rising edge?	Yes

Duty Cycle	***10%***

DDG	
Channel width	100 µs
Oscilloscope readings	
Period	1.00 ms
Frequency	1.00 kHz
Peak-Peak	2.72 V

VGEN GUI	
PRR	4.54 kHz

Photodiode	
Pulses seen?	Yes
In sync with signal rising edge?	Yes
~6 µs delay from rising edge?	Yes

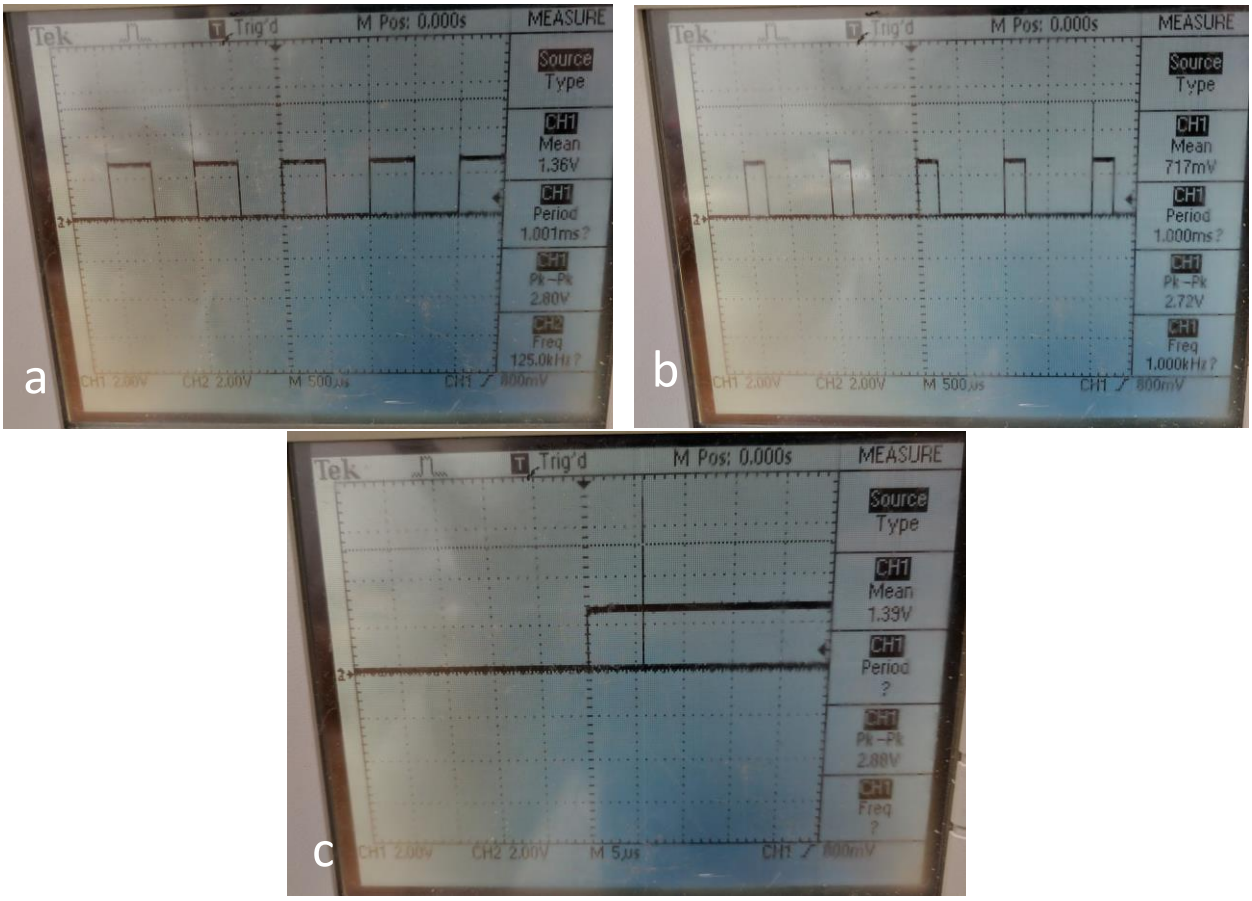

The above images are oscilloscope readings of the DDG and laser pulses at a frequency of 1 kHz, where image (a) shows the DDG pulses with pulse widths of 250 μs before turning the laser on, image (b) show the signal with the laser on, where the laser pulses can be seen at the rising edge of the DDG pulses, indicating that the DDG is triggering the laser. Image (c) shows a zoomed-in image of the rising edge of a DDG pulse with the triggered laser pulse signal detected about 6 μs after the rising edge.

OPNUM	**0**
Period	**100 µs**

Duty Cycle	***50%***
DDG	
Channel width	50 µs
Oscilloscope readings	
Period	100 µs
Frequency	10.00 kHz
Peak-Peak	2.80 V

VGEN GUI	
PRR	10.00 kHz

Photodiode	
Pulses seen?	Yes
In sync with signal rising edge?	Yes
~6 µs delay from rising edge?	Yes

Duty Cycle	***25%***
DDG	
Channel width	25 µs
Oscilloscope readings	
Period	100 µs
Frequency	10.00 kHz
Peak-Peak	2.88 V

VGEN GUI	
PRR	10.00 kHz

Photodiode	
Pulses seen?	Yes
In sync with signal rising edge?	Yes
~6 µs delay from rising edge?	Yes

Duty Cycle	***10%***
DDG	
Channel width	10 µs
Oscilloscope readings	
Period	100 µs
Frequency	10.00 kHz
Peak-Peak	2.88 V

VGEN GUI	
PRR	10.00 kHz

Photodiode	
Pulses seen?	Yes
In sync with signal rising edge?	Yes
~6 µs delay from rising edge?	Yes

Duty Cycle	***5%***
DDG	
Channel width	5 µs
Oscilloscope readings	
Period	100 µs
Frequency	10.00 kHz
Peak-Peak	2.80 V

VGEN GUI	
PRR	10.00 kHz

Photodiode	
Pulses seen?	Yes
In sync with signal rising edge?	Yes
~6 µs delay from rising edge?	Yes

Duty Cycle	***1%***
DDG	
Channel width	1 µs
Oscilloscope readings	
Period	100 µs
Frequency	10.00 kHz
Peak-Peak	2.80 V

VGEN GUI	
PRR	10.00 kHz

Photodiode	
Pulses seen?	Yes
In sync with signal rising edge?	Yes
~6 µs delay from rising edge?	Yes

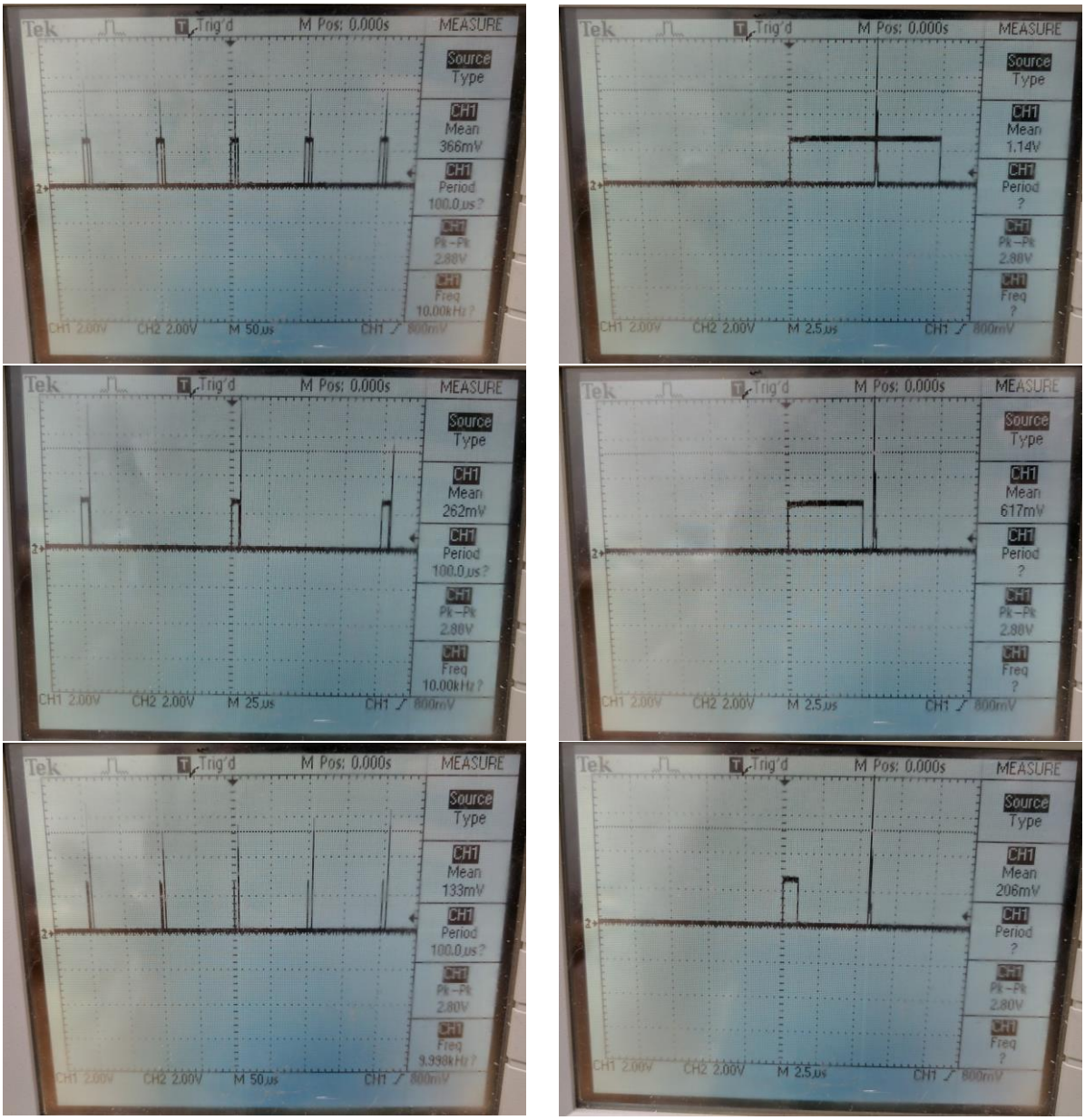

For the above set of images, the pulse widths were decreased from 10 µs to 5 µs to 1 µs (top to bottom). It is apparent that the laser pulse still occurs about 6 µs after the rising edge of the pulse sent by the DDG. However, since there no overlap between the laser pulses and the next signal sent by the DDG, the repetition rate was increased to 100 kHz and 178 kHz (maximum being 180 kHz) to see if the signal would clash and prevent pulses from emitting from the laser.

OPNUM	0
Period	10 µs

Duty Cycle	*50%*
DDG	
Channel width	5 µs
Oscilloscope readings	
Period	10 µs
Frequency	100.00 kHz
Peak-Peak	2.80 V

VGEN GUI	
PRR	100.00 kHz

Photodiode	
Pulses seen?	Yes
In sync with signal rising edge?	Yes
~6 µs delay from rising edge?	Yes

Duty Cycle	*10%*
DDG	
Channel width	1 µs
Oscilloscope readings	
Period	10 µs
Frequency	100.00 kHz
Peak-Peak	2.80 V

VGEN GUI	
PRR	100.00 kHz

Photodiode	
Pulses seen?	Yes
In sync with signal rising edge?	Yes
~6 µs delay from rising edge?	Yes

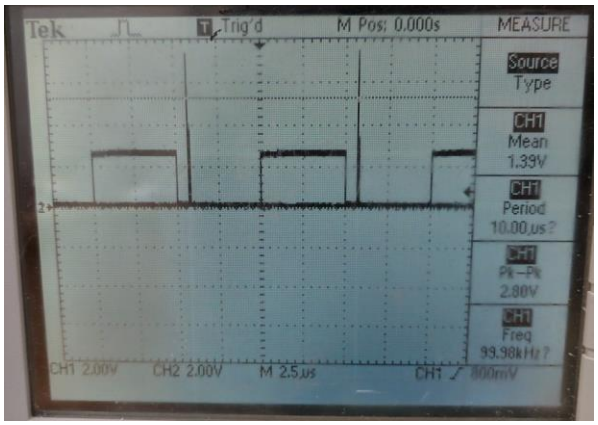

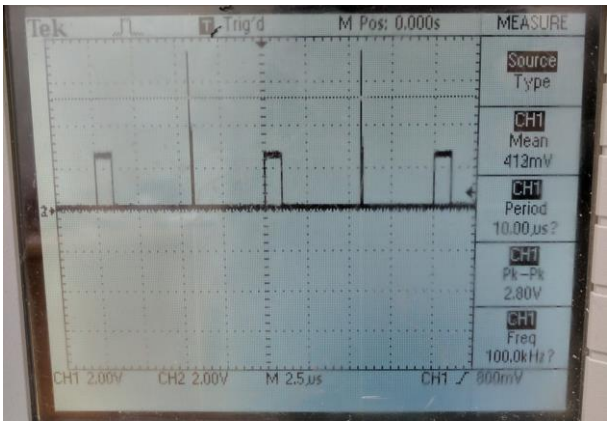

OPNUM	0
Period	**5.6 µs**

Duty Cycle	***45%***
DDG	
Channel width	2.5 µs
Oscilloscope readings	
Period	5.6 µs
Frequency	178.6 kHz
Peak-Peak	2.88 V

VGEN GUI	
PRR	178.72 kHz

Photodiode	
Pulses seen?	Yes
In sync with signal rising edge?	Yes
~6 µs delay from rising edge?	Yes

Duty Cycle	***18%***
DDG	
Channel width	1 µs
Oscilloscope readings	
Period	5.6 µs
Frequency	178.6 kHz
Peak-Peak	2.88 V

VGEN GUI	
PRR	178.72 kHz

Photodiode	
Pulses seen?	Yes
In sync with signal rising edge?	Yes
~6 µs delay from rising edge?	Yes



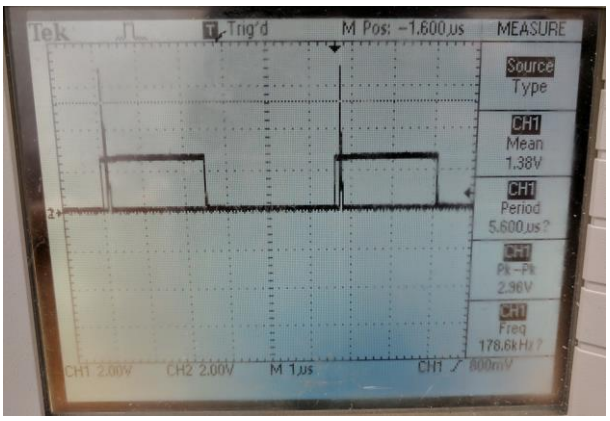

Note that with a higher repetition rate, one that is as close to maximum for OPNUM (180 kHz) as it was to use nice numbers with, the laser pulse is still about 6 µs after the rising edge of the initial signal sent by the DDG. However, the pulse overlaps that of the second signal sent by the DDG, as can be seen by the image on the right. Each horizontal division corresponds to 1 µs.